

UNIVERSITY OF BIRMINGHAM



UK
Quantum Technology Hub
Sensors and Timing

Reduction of Background Scattered Light for Future Compact Atom Interferometers

Hester Thomas, [redacted]

September 5, 2022

Supervisors: Dr M Holynski and Prof K Bongs
Post-doctoral Reseacher: Dr M Langlois

School of Physics and Astronomy
University of Birmingham
Birmingham, B15 2TT

Word Count: 10,616

UNIVERSITY OF
BIRMINGHAM

University of Birmingham Research Archive

e-theses repository

This unpublished thesis/dissertation is copyright of the author and/or third parties. The intellectual property rights of the author or third parties in respect of this work are as defined by The Copyright Designs and Patents Act 1988 or as modified by any successor legislation.

Any use made of information contained in this thesis/dissertation must be in accordance with that legislation and must be properly acknowledged. Further distribution or reproduction in any format is prohibited without the permission of the copyright holder.

Abstract

Atom Interferometry has exciting potential for use in gravity surveys which has many applications, for example in civil engineering. When doing field surveys, a compact system is highly valuable; a system needs to be moved and operated by one person and last for a day of measurements operating on battery power. A compact cold atoms system is built; the final system has a weight of 17 kg, a power of 125 W and a volume of 45 l meeting the objective of < 20 kg, < 150 W and < 100 l. The system currently operates using a bench power supply not accounted for in the volume, a compact power supply has been built and is now being tested. A cloud of cold rubidium atoms is formed in the magneto optical trap, trapping 1.2×10^8 atoms with a loading time of 0.7 s and with a typical error of approximately 5%. This is the first step in realising a compact atom interferometer. Due to the size of the compact system any noise contributions become more significant; one way of addressing this is in reducing the contribution of scattered background light to the signal to noise and signal to background ratios. A new method of using anodised titanium to realise a blackened coating while constructing the vacuum chamber of the MOT is investigated; the reflectance of this coating is investigated and compared to that of uncoated titanium. It is found that the reflectance of light is reduced by the PCO35 coating across all investigated wavelengths, proving the PCO35 coating to be significantly less reflective than the uncoated titanium. The coating is tested in a vacuum chamber where no significant outgassing is observed, it is then used in a test prism MOT to asses compatibility with rubidium vapour; there is a possible noise reduction of 23% compared to an uncoated test system. The chamber was kept at UHV pressure for over a year and no degradation of the coating was observed. The suitability and advantages of using the PCO35 coating in a cold atoms system have been

assessed and the PCO35 coating is available as a technology choice for future quantum sensor systems.

Contents

1 Introduction **3**

2 A Compact Gravity Gradiometer **7**

2.1 Theory 7

2.1.1 Laser Cooling 7

2.1.1.1 Doppler Cooling 8

2.1.1.2 The Magneto Optical Trap 10

2.1.1.3 Optical Molasses – Cooling Below the Doppler Limit 13

2.1.2 Preparation of the Atom Cloud 16

2.1.2.1 Velocity Selection 16

2.1.2.2 Magnetic State Selection 17

2.1.3 Atom Interferometry 17

2.1.3.1 Raman Pulses 17

2.1.3.2 Measurements of gravity 19

2.1.3.3 Gravity Gradiometry 20

2.2 Experimental Design of the compact gradiometer 22

2.2.1 The Vacuum System 23

2.2.2 The Laser System 25

2.2.2.1 Frequency Generation 25

2.2.2.2 Integration into the Laser System 26

2.3 Build of the Experiment and First Results 30

2.3.0.1 Building the Vacuum system 31

2.3.0.2 Characterisation measurements of the Laser System 33

2.3.1 Generation of Cold Atoms in the MOT 34

2.4 System Status 35

3 The Reduction of Scattered Background Light in Cold Atom Vacuum Systems 37

3.1 Introduction 37

3.2 Characterisation of the PCO35 coating in a vacuum 38

3.2.1 Theory 38

3.2.2 The Test Vacuum System 39

3.2.3 Measurements 42

3.3 Characterisation of optical properties 45

3.3.1 Theory 45

3.3.2 Experimental Set-Up 46

3.3.3 Measurements 47

3.4 The use of the PCO35 coating in a Cold Atom Vacuum System 49

3.4.1 Construction of the test chamber 49

3.4.2 Comparison between a coated and uncoated test chamber when producing a cold atom cloud 50

4 Conclusion 53

Acknowledgments 55

1. Introduction

Atom interferometry is a quickly growing field, based on the 1991 work of Mark Kasevich and Steve Chu who introduced light-pulse atom interferometry using stimulated Raman transitions [1] [2]. Atom interferometry is analogous to a classical light interferometer with the roles of light and matter reversed: using a cloud of cold atoms as a test mass and measuring the phase difference across the interferometer [3]. Since its introduction, atom interferometry has become a wide field [4]: it opens the door for detailed tests of the fundamental laws of physics, including measurements of newtons gravitation constant, big G [5]; measurements of the fine structure constant α as a test of the standard model [6]; testing the pillars of general relativity by measuring the universality of free fall posed by Einstein's equivalence principle [7] [8]; and more recently, proposing applications in detecting gravitational waves [9]. Furthermore, atom interferometry allows for numerous applications in inertial sensing: it is possible to measure the rotation of the atoms, which allows for precise measurements of the rotation of the Earth among other applications [10]; and by measuring the acceleration of an atom cloud, it is possible to measure a highly precise value of the local gravitational field [11] [12], or indeed of the local gravity gradient [13].

Since atom interferometry was first demonstrated, cold atoms based atom interferometry has given the most precise measurements of the local gravity to date, with measurements to a precision of 6.7pg [12]. Using density contrast measurements, it becomes possible to use cold atoms based gravimetry to detect features that are underground; taking measurements of the local gravity signal while moving the atom interferometer over an area can find a feature — for example a tunnel or pipeline — under the ground due to their density contrast, as shown in figure 1.1. This allows for wider applications in geophysical sensing [14] [15], for example transport and construction. Currently, portable gravimeters are typically based on a mass-spring approach; ground penetrating radar systems are an alternate technology that

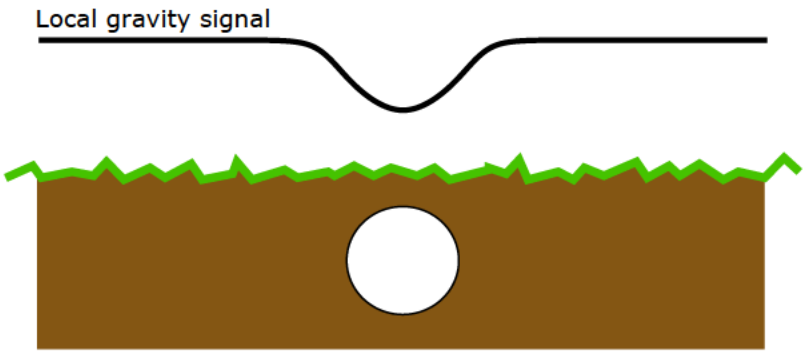


Figure 1.1: An illustration of how a structure underground affects the local gravitational field due a difference in density in materials.

is also used to detect underground features. Compared to these systems, atom interferometry based gravimetry can detect features at a greater depth, at the cost of a longer measurement time [16]. The Innovate UK Sigma project predicts that a new atom interferometry based system could provide enhanced detectability; allowing for measurements of either features at twice the depth at a given object radius, or measurements of half the object radius at a given depth compared to current methods [17].

To be viable to field applications, an atom interferometry system must be able to compete with the existing commercial gravity sensors [14] [15] [18]. Cold atoms systems already pose several potential benefits over mechanical gravity sensors including increased precision in measurements and the ability to be run continuously — as they don't use mechanical moving parts, there is no worry about mechanical wear of the system, significantly improving its lifetime [19]. However, in field surveys the typical operation of a gravity sensor requires the device to be frequently moved and operated often by a single person, as well as taking measurements over the course of a day using battery power. Although significant improvements have been made in recent years in portable and robust atom interferometry systems [16] [20] [21], the existing cold atoms based gravity sensors are large and cumbersome compared to the existing commercial sensors. Furthermore, there are applications to mount the compact

gravity sensor on a UAV (unmanned aerial vehicle), opening a new range of possibilities for measurements. When taking measurements in the air, it becomes possible to survey areas where one could not access by foot, for example a cliff edge, or an area with improvised explosive devices (IEDs) of unknown locations.

Therefore, to be competitive in the field of commercial gravity sensors, work must be done to reduce the size, weight and power consumption of the atom interferometer. Effort is made to make a atom interferometer under the size, weight and power constraints of < 100 l, < 20 kg and < 150 W respectively, making a system that can be moved and operated by a single person. This is achieved using innovative techniques such as when constructing the laser system. In this case, two IQ Modulators to generate all the required laser frequencies for an atom interferometry sequence using a single laser seed, discussed in section 2.2.2, creating a compact and robust cold atoms based gravimeter, with potential to become a gravity gradiometer at no cost to the size of the system.

Finally, gravity sensing using any method is susceptible to noise in the system and in the environment; it is important to understand and suppress sources of noise where possible. One particular source of noise that has yet to be addressed is from background scattered light from the incident lasers, that contributes to the detected light in the system and decreases both the signal to noise and signal to background ratios. To reduce the noise from scattered light a new technique is investigated, with the research into this method being published in API Advances, under the title "Reduction of background scattered light in vacuum systems for cold atoms experiments" [22]: using a "blackened", or absorptive, coating on the inner surfaces of the vacuum chamber housing a cold atoms system. The commercially available PCO35 coating [23] is tested to assess the benefits it provides to cold atom sensors, while also assessing its viability in an ultra high vacuum (UHV) environment and whether it is influenced by rubidium in a UHV chamber. Through this work, the coating is found to significantly reduce background scattered light, and it is used to construct a magneto-optical

trap; the coating is found to be both useful for and applicable to quantum sensors.

2. A Compact Gravity Gradiometer

2.1 Theory

When building a cold atoms system to take measurements of the local gravity gradient, many processes are required such as the laser cooling and trapping of atoms — to get precise measurements, cold atoms are vital; this will prevent the cloud of cold atoms from quickly expanding and dispersing, allowing for a longer measurement time [21]. After cooling and trapping atoms in a magneto-optical trap and optical molasses, the atom cloud is prepared for an atom interferometry sequence using a velocity and magnetic state selection process; finally, an atom interferometry sequence is followed.

2.1.1 Laser Cooling

Laser cooling makes use of the transfer of momentum to an atom when it absorbs a photon. When an atom with velocity v absorbs a photon with wavelength ω it receives a momentum change of $\hbar k$ in the direction of the laser beam. If the direction of the laser is opposing that of the atom, this works to slow the atom. The atom then spontaneously emits a photon in a random direction. Over a series of absorption and spontaneous emission events the contribution to the momentum of the atom from emission of a photon averages towards zero, as shown in figure 2.1. This gives a net force on the atom equal to $F = \rho_{ee}\hbar k\Gamma$ in the direction of the laser, where $\rho_{ee} = \frac{1/2s}{1+s+(2\delta/\Gamma)^2}$, δ is the detuning, $s = I/I_{sat}$ is the saturation parameter and Γ is the natural linewidth of the transition [3] [24]. In the limit of high intensity, $\rho_{ee} = 1/2$ and $F = \hbar k\Gamma/2$. This process works when cooling a beam of atoms travelling in the opposite direction to a laser. When working with a rubidium vapour where atoms are moving in all directions, further cooling techniques are required.

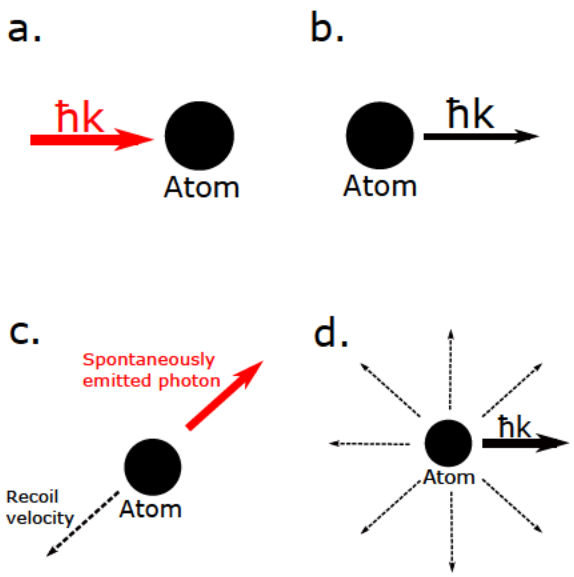


Figure 2.1: Laser cooling an atom. a) a photon with energy $\hbar k$ is incident on an atom; b) the atom absorbs a photon and gains a momentum of $\hbar k$; c) the atom spontaneously emits the photon, and experiences a recoil momentum in the opposite direction; d) over time, the atom absorbs and spontaneously emits many photons, the net average of the recoil velocities is zero and the atom gains a net momentum in the direction of the laser.

2.1.1.1 Doppler Cooling

In a vapour, atom cooling is needed in all directions; first, consider a two-dimensional case. A pair of counter-propagating lasers are used, each incident on the atoms. As an atom is moving it will see a photon's frequency Doppler shifted away from its frequency in the laser's rest frame, with the frequency being blue-shifted when the atom and the laser are counter-propagating, and the frequency being red-shifted when the atom and the laser and co-propagating, as shown in figure 2.2. Making use of this effect, the laser frequency is detuned below the atomic resonant frequency; this results in atoms predominantly absorbing photons that oppose their direction of travel, thus cooling the atoms with a damping, or viscous, force $F = -\alpha v$ [3] [25]. Initially, the atoms are moving at different velocities and have a wide velocity distribution that is centered on $v = 0$; laser cooling narrows the velocity spread of the atoms, cooling them. Introducing pairs of counter-propagating laser beams along the

three Cartesian axes cools the atoms in three-dimensions.

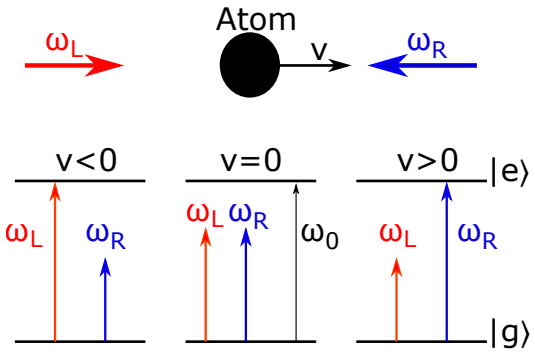


Figure 2.2: One dimensional Doppler cooling. The frequency of the incident light is detuned to be slightly lower than the resonant frequency of the atom; when the atom is travelling towards the laser beam it sees a frequency that is blue-shifted towards the atomic resonant frequency, such that the atoms predominantly absorb photons that oppose their direction of travel.

The laser cooling process works due to the heating effect of photon emission averaging to zero. However this still has an effect on the temperature that can be reached using the Doppler cooling method. The heating rate is proportional to the photon scattering rate due to the finite linewidth, Γ, of the transition; this is independent of velocity at low temperatures. Meanwhile, the cooling rate is proportional to the kinetic energy of the atoms. At the equilibrium point between these two effects no further cooling can be achieved, giving the Doppler limit on temperature to be

$$T_{\text{Doppler}} = \hbar\Gamma/2k_B, \tag{2.1}$$

where Γ is the natural linewidth of the transition of interest and k_B is the Boltzmann constant. In the case of rubidium-87, $\Gamma = 2\pi \times 6.065$ MHz for the cooling transition. This gives $T_{\text{Doppler}} = 145.57\ \mu$K [26].

2.1.1.2 The Magneto Optical Trap

The Doppler cooling process only works to cool the atoms, a second process is required to add a spatial dependence to the cooling force and trap the atoms. To achieve this, a magneto optical trap (MOT) is used, which relies both on the Doppler cooling process, and on the Zeeman splitting of energy levels.

In a magnetic field, the hyperfine levels of rubidium further split into magnetic hyperfine (m_F) states; the separation between the m_F states to first order changes linearly with the magnetic field, as shown in figure 2.4. Therefore, due to the Zeeman effect, in the presence of a linearly varying magnetic field, the magnetic sub-levels of an atom will linearly vary with the atom's position. The magnetic field is created by using a pair of anti-Helmholtz coils to create a minimum at the centre of the trap, shown in figure 2.3.

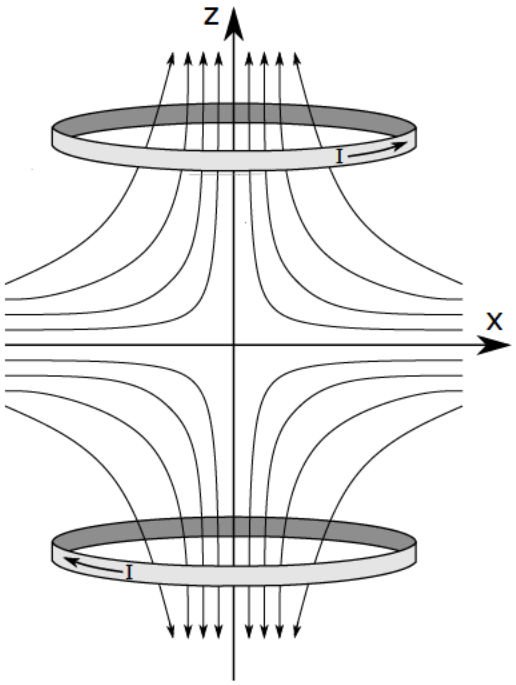


Figure 2.3: A pair of coils with a current I in anti-Helmholtz configuration generate a quadrupole magnetic field. The field is zero at the centre of the coils and increases linearly in every direction from the centre of the coils [3].

Counter-propagating laser beams incident on the atoms in the trap are detuned so that the frequency of the light is lower than the atomic resonance frequency, as in the Doppler cooling process. This combined with the quadrupole magnetic field adds a spatially dependent imbalance in the scattering forces on the atoms and confines them in the centre on the trap. For illustrative purposes, consider an atom being driven between the $J = 0$ and $J = 1$

states. The atom is displaced to the right of the trap such that $z > 0$, where $m_J = -1$ moves closer to the atomic resonance frequency as shown in figure 2.4; selection rules dictate that σ^- light excites the $m_J = -1$ sub-level. When the laser beam incident on the atoms from the right is σ^- circularly polarised, the scattering force on the atom pushes it towards the centre of the trap. Likewise for $z < 0$, σ^+ circularly polarised light excited the $m_J = +1$ sub-level and the scattering force on the atom pushes it towards the centre of the trap. This imbalance in radiation force results in a position dependent restoring force on the atoms, causing them to undergo over-damped simple harmonic motion in the presence of the magnetic and light fields. The MOT has a large capture volume, allowing atoms to be captured from a room temperature vapour [3].

The MOT cools and traps atoms from the rubidium vapour in the chamber, and it loads atoms as

$$N(t) = N_0(1 - e^{-t/\tau}) \tag{2.2}$$

where N_0 is the saturated atom number in the MOT and τ is the loading time of the trap. By measuring the number of atoms loading in the MOT over time, the loading time of the trap can easily be determined; for a given MOT geometry, this should only be affected by the background gas pressure, the density of the rubidium vapour and the rubidium atoms' speed at room temperature.

When atoms are trapped in the MOT, they fluoresce due to the process of continually absorbing and emitting photons. By measuring this fluorescence the number of atoms can be measured.

$$N = \frac{V}{eR_s\Omega QR} \tag{2.3}$$

The fluorescence is measured using a photodiode with a solid angle of Ω, a quantum efficiency of Q and a gain resistance of R. V is the voltage drop over the photodiode when

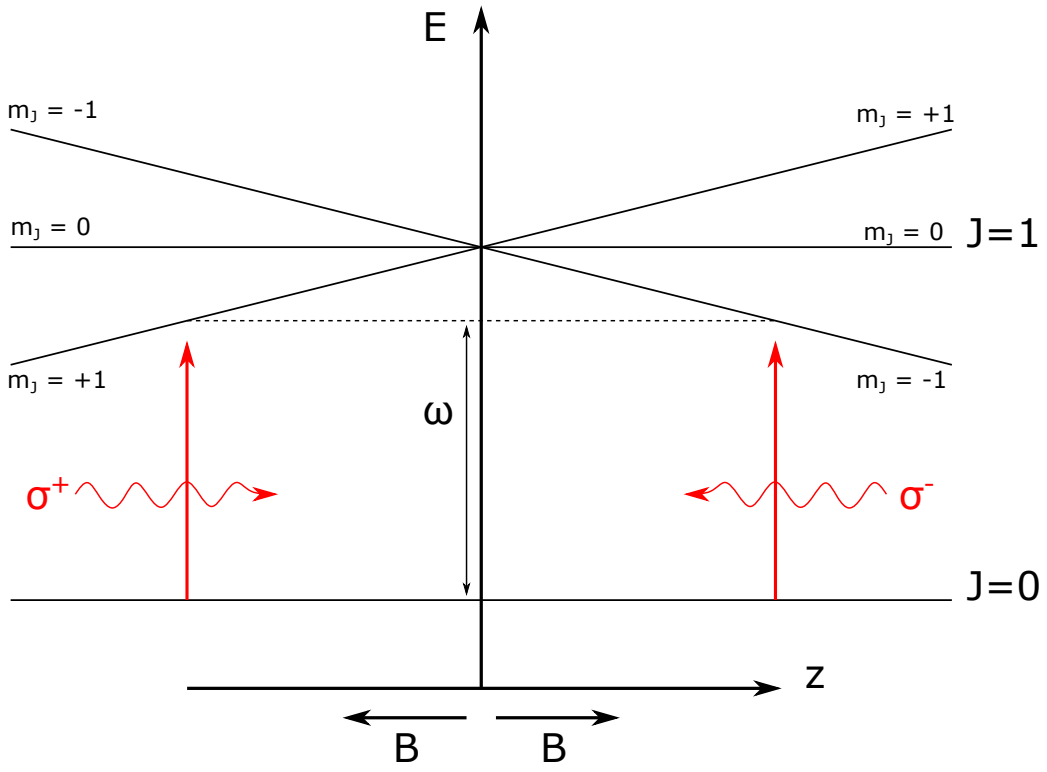


Figure 2.4: An illustration of the mechanics behind a magneto-optical trap (MOT) for an atom moving between the J=0 and J=1 energy levels. In the presence of a linearly varying quadrupole magnetic field, the J=1 sublevel splits into three magnetic sub-states ($m_J = 0, \pm 1$), whose separation increases linearly from the centre of the trap. A pair of counter-propagating circularly polarised laser beams illuminate the atoms in the trap causing an imbalance in the radiative forces leading to the atoms experiencing over-damped simple harmonic motion.

measurements are taken, e is the electron charge, and R_s is the photon scattering rate [25].

When considering a multi-level atom such as rubidium, to prevent atoms from being "lost" during the Doppler cooling process a repump laser beam is also used. The cooling laser drives transitions from $|F = 2\rangle \rightarrow |F' = 3\rangle$, however this cooling laser also has a finite probability of driving a transition from $|F = 2\rangle \rightarrow |F' = 2\rangle$; when this happens the atom can decay to the $|F = 1\rangle$ "dark" state. The cooling laser is not at the correct frequency to excite atoms from this hyperfine state. The repump laser is introduced to excite these atoms from

$|F = 1\rangle \rightarrow |F' = 2\rangle$ as shown in figure 2.5; from $|F' = 2\rangle$ the atoms have a probability of decaying to $|F = 2\rangle$ where they will re-enter the cooling process. This prevents atoms from being lost from the cooling cycle [25].

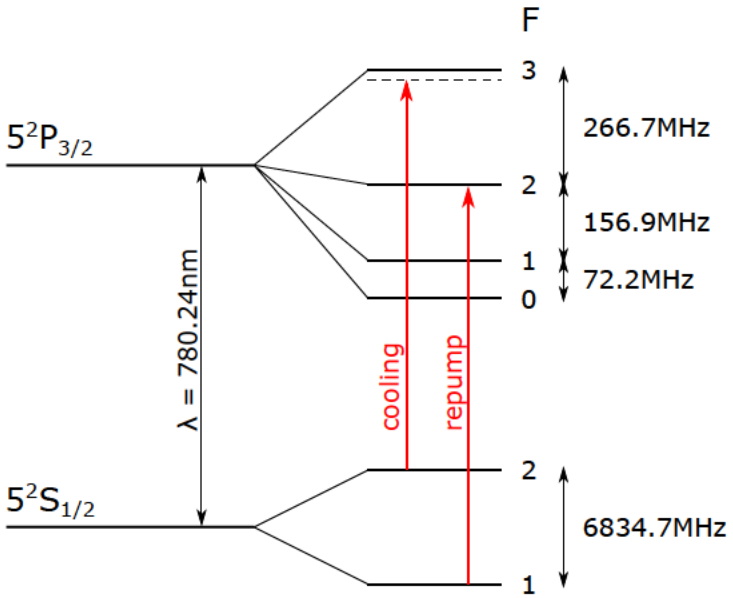


Figure 2.5: The hyperfine structure of the D2 line of rubidium-87, showing both the cooling and repump transitions [26].

2.1.1.3 Optical Molasses – Cooling Below the Doppler Limit

A temperature of $T_{\text{Doppler}} = 145.57\ \mu\text{K}$ can be reached in the MOT using the Doppler cooling method for rubidium-87 [26]; to perform atom interferometry, the atom cloud must be further

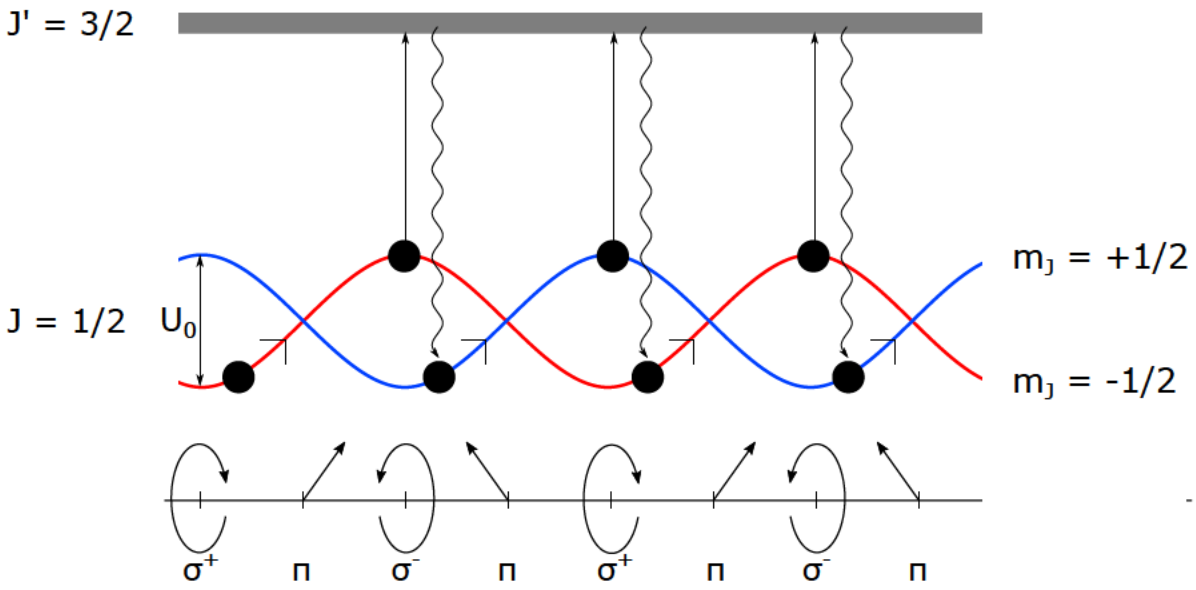


Figure 2.6: An illustration of the process of Sisyphus cooling

cooled so that the atom cloud does not expand significantly over the measurement period. This is done using a sub-Doppler cooling techniques. One example of these is Sisyphus cooling, which is possible due to the multi-level structure of the atom.

With pairs of counter-propagating laser beams a standing wave is formed. The beams have σ^+ and σ^- polarisation, and the resulting polarisation of the standing wave varies with position, dependent on the relative phase of the two beams. An atom in a standing wave with varying polarisation will experience two effects: light shift and optical pumping. Each magnetic sub-level will be shifted with the varying polarisation, resulting in the two m_J ground-states varying sinusoidally with position in the standing wave, as shown in figure 2.6 [3].

Optical pumping is a process through which light transfers a population of atoms into a specific state. Take an atom in the $\mathrm{m_J} = -1/2$ ground state, being illuminated with σ^+ light. This atom will excite to the $\mathrm{m'_J} = +1/2$ excited state, and after some short time it

will spontaneously emit a photon and drop down to either the $m_J = -1/2$ or $m_J = +1/2$ ground states. For the latter case, the atom in the $m_J = +1/2$ ground state can be excited to $m'_J = +3/2$ with σ^+ light; after emitting a photon, this atom can only de-excite back to $m_J = +1/2$, there is no path back to $m_J = -1/2$ and it is stuck. Following this process, atoms will move from $m_J = -1/2$ to $m_J = +1/2$ via an excited state. The reverse is also true for σ^- light, with atoms moving from $m_J = +1/2$ to $m_J = -1/2$.

In Sisyphus cooling, with a configuration shown in figure 2.6, an atom will travel along the varying potential, converting kinetic energy into potential energy and vice versa. An atom in the $m_J = -1/2$ ground state climbs the "hill" of the potential, reaching the top where it is illuminated with σ^+ polarised light. This atom is then optically pumped into the $m_J = +1/2$ state where it finds itself in a "valley" of the potential, having lost energy roughly equal to the separation between the maxima and the minima of the varying potential, U_0 [3]. The atom climbs a hill and falls back down, over and over again, slowly losing energy as it goes; this process is what lends this cooling technique a name, as it can be likened to the Greek myth where Sisyphus is cursed to forever push a boulder up a hill, only for it to fall back down every evening.

Sisyphus cooling continues until the atom no longer has the energy to climb the "hill", i.e. $k_B T \approx U_0 \propto \frac{I}{|\delta|}$. The laser detuning, δ, is slowly increased while the intensity, I, is decreased, this decreases U_0 and allows Sisyphus cooling to continue, reaching lowing temperatures. This continues until the recoil temperature is reached when the loss in energy from climbing the "hill" and falling back down, U_0, is balanced by the recoil energy from the spontaneous emission of a photon. This gives a limit on the minimum temperature as

$$T_{\text{recoil}} = \frac{\hbar^2 k^2}{m k_B} = \frac{h^2}{m k_B \lambda^2} \tag{2.4}$$

where k and λ are the wave number and wavelength respectively for transition, shown for

the D2 transition of rubidium-87 in figure 2.5, and m is the atomic mass. For rubidium-87, $T_{\text{recoil}} = 361.96$ nK [26]. In practise, this limit is rarely reached, this can be due to background magnetic fields [3]. Temperatures that are orders of magnitudes lower than T_{doppler} are still reached, with a goal of 5 μK.

2.1.2 Preparation of the Atom Cloud

There are several conditions, in addition to the cooling of the atom cloud discussed in section 2.1.1, that must be met for atom interferometry to be performed. The atoms need to have a narrow velocity range centered over $v = 0$ and they are typically put into the $\text{m}_\text{F} = 0$ magnetic sub level to reduce their dependence on magnetic fields.

2.1.2.1 Velocity Selection

Raman pulses have a Fourier limited linewidth, thus they only interact with atoms with a very small velocity range; to achieve a high signal to noise ratio the interferometer must address as many atoms as possible, this is done by cooling the atoms such that as many atoms as possible are in this velocity class and selectively removing those which are not. The initial width of the atoms velocity distribution is first narrowed using a far detuned, low intensity optical molasses, as discussed in section 2.1.1.3. To then select only atoms with the desired velocity range, a long Raman pulse is used, transferring atoms from $|\text{F} = 2\rangle$ to $|\text{F} = 1\rangle$. This Raman pulse has a width at $1/\sqrt{e}$ of $\sigma_t = 1/2\pi\sigma_\nu$ in the time domain; this pulse therefore only addresses atoms over a velocity distribution $\sigma_v = \sigma_\nu c/2\nu_{\text{laser}}$. This selected velocity range corresponds to a temperature of

$$T = \frac{m\sigma_v^2}{k_B} \tag{2.5}$$

where m is the atomic mass. All atoms that are not selected remain in the $|\mathrm{F}=2\rangle$ state and a blow away pulse corresponding to $|\mathrm{F}=2\rangle \rightarrow |\mathrm{F}'=3\rangle$ pushes these faster atoms to the walls of the vacuum chamber [27][20].

2.1.2.2 Magnetic State Selection

To reduce any Zeeman shift in the energy levels of the atoms while in the presence of a magnetic field, either from the interferometer system or from stray magnetic fields, the $\mathrm{m_F} = 0$ magnetic sub-level must be used. This is especially relevant when considering a portable system for field applications. For magnetic state selection, a microwave RF pulse is used to transfer atoms from $|\mathrm{F}=1,\mathrm{m_F}=0\rangle$ to $|\mathrm{F}=2,\mathrm{m_F}=0\rangle$; all atoms that were not in the $m_F = 0$ sub-state are left in the $|\mathrm{F}=1\rangle$ state and later removed using a blow away pulse corresponding to $|\mathrm{F}=1\rangle \rightarrow |\mathrm{F}'=0\rangle$. As there are three magnetic sub-states in $|\mathrm{F}=1\rangle, (\mathrm{m_F}=0,\pm 1)$, this results in a loss of two thirds of the atoms [20].

After this process, all atoms are in the $|\mathrm{F}=2,\mathrm{m_F}=0\rangle$ state, with a narrow velocity range determined by equation 2.5, allowing for high sensitivity and minimal loss in contrast during the interferometry sequence.

2.1.3 Atom Interferometry

2.1.3.1 Raman Pulses

A Raman beam consists of two counterpropagating laser beams with frequencies ω_1 and ω_2 which drive a transition between two states using the simultaneous absorption and stimulated emission of a photon by an atom. This is analogous to a single beam transition with frequency ω_{12}, but with the following benefits: The Raman transition has a very narrow linewidth, therefore a long lifetime — it puts the atom into a meta-stable ground state so that there's no spontaneous emission between the interferometer pulses; additionally, a counter-propagating

Raman transition provides two photon recoils, giving a larger opening of the interferometer [2][3][20].

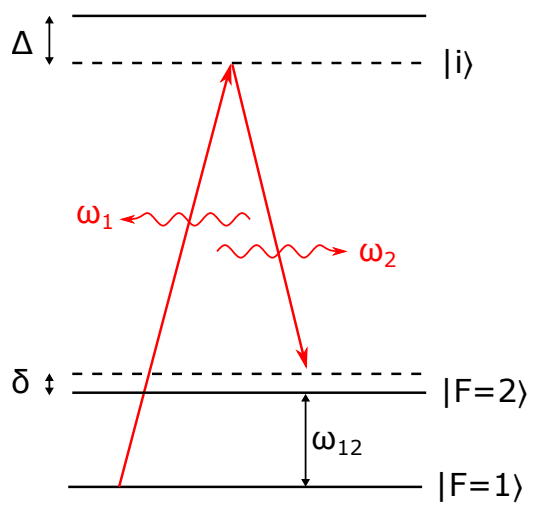


Figure 2.7: Stimulated Raman transitions between the F=1 and F=2 hyperfine states of rubidium.

Raman transitions couple the $|\mathrm{F}=1\rangle$ and the $|\mathrm{F}=2\rangle$ hyperfine states via an intermediate state; provided the two photon detuning of this state, δ, is significantly larger than the single photon detuning, Δ and the linewidth of the intermediate state, $|i\rangle$, this intermediate state is never populated and the system can be treated as a near-perfect two-level system with negligible decay. This effective two level system has resonant frequency, $\omega = \omega_{\mathrm{eff}} - \delta$ and momentum difference between levels $= \hbar k_{\mathrm{eff}}$ where the effective frequency and wave number are given by

$$\omega_{\mathrm{eff}} = \omega_1 - \omega_2 \approx \omega_{12} \tag{2.6}$$

$$k_{\mathrm{eff}} = k_1 - k_2 \approx 2k_1 \tag{2.7}$$

for a counter-propagating beam configuration [20].

When a Raman pulse is applied to a population of atoms, Rabi oscillations are driven between the two states of the system. The atoms in the system cyclically absorb and re-emit photons in the presence of a Raman beam; the rate at which this process occurs is given by the Rabi frequency, Ω_R. This can in turn be used to dictate the ratio of atoms in the $|\mathrm{F}=1\rangle$ and $|\mathrm{F}=2\rangle$ states. The Rabi frequency is first determined by measuring the ratio of the two states as the length of the Raman pulse is varied. Once known, the length of the

Raman pulse is used to controll the ratio of atoms. Two particular cases are of interest: a $\pi/2$ Raman pulse of length τ which is used to split atoms into a 50:50 superposition of the two states, where $\tau\Omega_R = \pi/2$; and a π Raman pulse of length τ which is used to invert the states of the atoms, where $2\tau\Omega_R = \pi$ [3].

2.1.3.2 Measurements of gravity

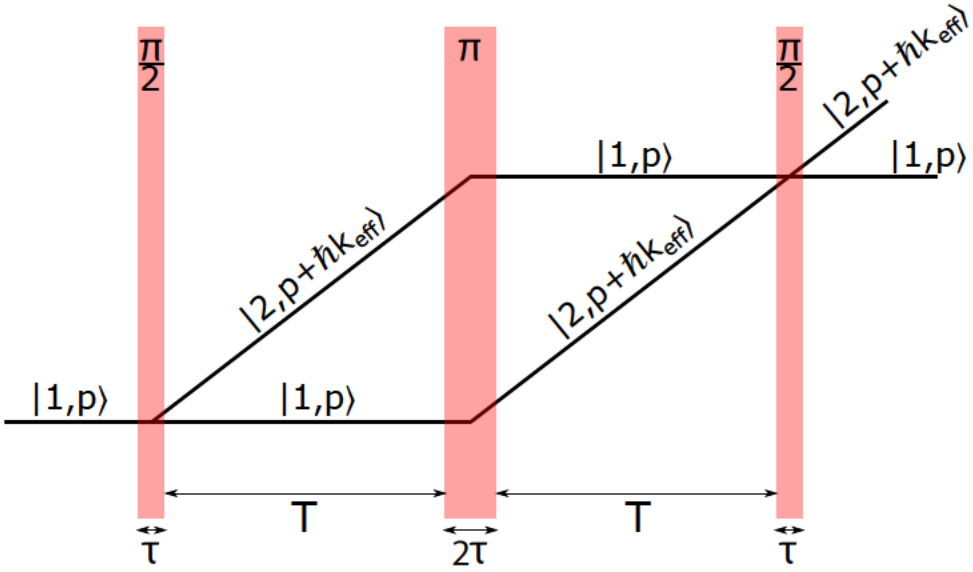


Figure 2.8: An atom interferometer consisting of a $\pi/2, \pi, \pi/2$ sequence. These Raman pulses are used to split, invert an recombine the atoms and a measurement of the populations of atoms in the ground and excited states is taken at the output of the interferometer.

In an atom interferometer, one possible interferometry sequence uses three Raman pulses to split, reflect, and recombine a population of atoms, as shown in figure 2.8. Between each of these pulses, the atoms are allowed to freely evolve for time T. At each of these pulses, a momentum change is imparted to a portion of the atomic wave funtion, given by $\hbar k_{\text{eff}}$.

The atoms experience a difference in path length across the interferometer, due to their acceleration due to gravity. This phase difference across the interferometer determines the

population ratio at the output of the interferometer, Φ. This is called the total interferometer phase, and can be separated in to two components, the phase difference due to the atoms' interaction with the Raman pulses, ϕ_{int}, and the phase difference due to the free evolution between pulses, ϕ_{evol}, such that

$$\Phi = \phi_{\text{int}} + \phi_{\text{evol}}. \tag{2.8}$$

The phase difference across the interferometer due to the interaction with the Raman pulses is given by $\phi_{\text{int}} = k_{\text{eff}} gT(T + 2\tau) + \Delta\phi_{\text{offset}}$; meanwhile, as the interferometer is symmetrical, the phase difference from the free evolution of the atoms cancels out across the interferometer, and $\phi_{\text{evol}} = 0$. Therefore the total interferometer phase is given by

$$\Phi = k_{\text{eff}} gT(T = 2\tau) + \Delta\phi_{\text{offset}} [20]. \tag{2.9}$$

To measure the actual value of the local gravity, the Raman beam frequency is chirped at rate α; this is done to compensate for the atoms' acceleration and the subsequent change in Doppler shift in the laser frequency as they fall due to gravity. As the chirp rate is varied, the ratio of populations of the two states varies sinusoidally. This process is repeated over several T times between Raman pulses, as shown in figure 2.9, and there is one value of chirp rate, α_0 for which the phases is independent of the T time.

Using this value of the chirp rate, α_0, for an ideal case the value of local gravity is found to be

$$|g| = \frac{2\pi\alpha_0}{|k_{\text{eff}}| cos(\theta)} \tag{2.10}$$

where θ is the angle between the local gravity vector and the axis of the Raman beams [20].

2.1.3.3 Gravity Gradiometry

Due to Einstein's equivalence principle, when making a measurement of gravity it is impossible to distinguish gravitational acceleration experienced by the test cloud of atoms,

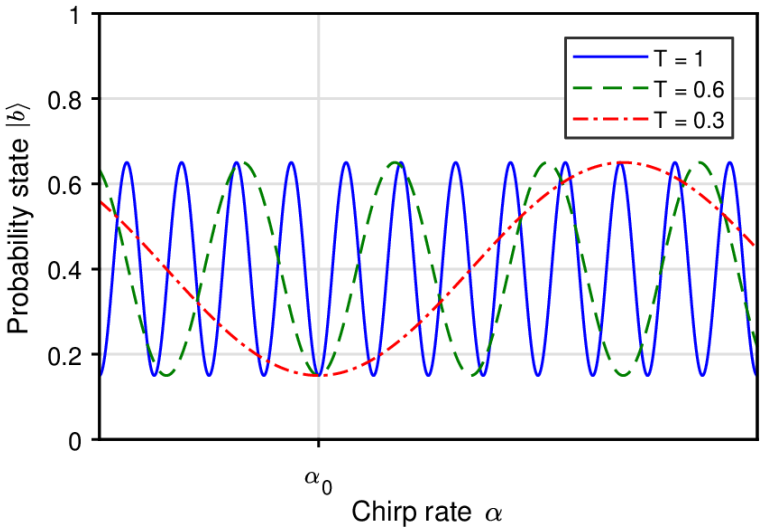


Figure 2.9: The probability of atoms being in the $|2\rangle$ state after an interferometry sequence as a funtion of the chirp rate, with T given in ms [21].

and the acceleration of the reference frame. The reference frame of the atom interferometer will accelerate due to vibrations or movement of the instrument; this makes the the gravity measurements performed very susceptible to external noise caused by vibration.

When two atom clouds are used to perform simultaneous atom interferometry sequences while spatially separated by a known distance, as shown in figure 2.10, it becomes possible to measure the gravity gradient. Using a common laser beam couples the measurements; when taking coupled measurements made in the same reference frame, any external vibration results in the two atom clouds experiencing common acceleration; thus all external acceleration of the reference frame is common-mode and can be removed as such [28]. Using this same principle, other sources of noise that affect both gravity measurements, such as tilt of the Raman beams with respect to the gravity gradient, can also be suppressed as common-mode. For gradiometers where the two atom clouds experience the same vibration, for example when the atom clouds are both in free fall, and where a common laser is used to perform coupled measurements, this significantly reduces the noise on gravity gradiometry measurements compared to gravimetry measurement. This makes the gravity gradiometer

well suited for field applications. Gravity gradients can be used to measure large differential mass distribution, for example a large cavity or deposit underground.

2.2 Experimental Design of the compact gradiometer

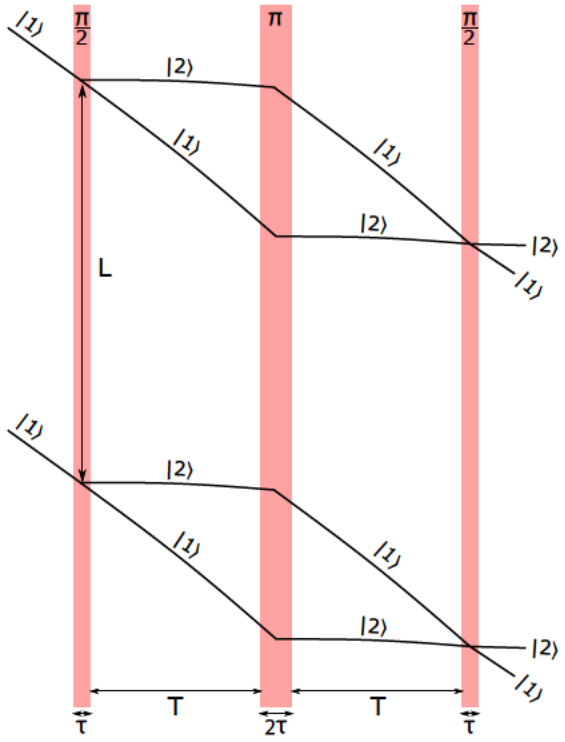


Figure 2.10: A gravity gradiometer consisting of two atom interferometry sequences, performed simultaneously while spatially separated by distance L.

To be useful in commercial applications, the system must be compact and portable, with the potential of being operated remotely while flying on a UAV (unstaffed aerial vehicle). To achieve this goal, the system must be designed and built with consideration of the weight, size and power of the system, with constraints of $<$ 20 kg, $<$ 100 l and $<$ 150 W respectively. When designing a compact system, novel methods must be employed to facilitate the necessary reduction in size, weight and power. The vacuum system is designed so that a single atom cloud is formed initially, it will then be split and separated to form the two atom clouds used in gravity gradiometry. The vacuum system is also designed to be physically small so that it can fit in a small cylindrical magnetic shield, reducing the weight of the magnetic shield used to negate the effects on stray magnetic fields that may be present around the system. An agile laser system is used to reduce the power of the system, with care taken to limit the number of components that have a high power consumption, such as acousto-optical modulators (AOM) and

erbium doped fibre amplifiers (EDFA). Furthermore, the design should be modular such that each section: laser system, controls, power distribution, and microwave chain, are separate. This allows for easy assembly and disassembly when setting up the experiment, and when diagnosing and fixing faults in the experiment.

Significantly reducing the size of a system, as is done here, comes at an initial cost of worsening the signal to noise and signal to background ratios. This is for several reasons: the system has a finite baseline due to its length — when sensitivity in the system depends on the separation between the two atom clouds in the gradiometer, with greater separation giving a greater sensitivity, this puts a fundamental limit of the sensitivity of the system; additionally, the system is limited in the time, T, between interferometer pulses, as this is dependent on how far the atoms can fall or be launched. Furthermore, the small size of the system may limit the number of atoms in the atom cloud. Even is not the case, due to the small size of the system, instead of simultaneously creating two atom clouds to perform the two atom interferometry sequences required for gravity gradiometry, as is done in larger systems [29], one atom cloud is instead formed and split into two atom clouds; this allows for a much more compact system at the cost of fewer atoms in each atom interferometry region of the gradiometer. All of these factors affect the shot noise of the system, thus work must be done to reduce other sources of noise and improve the precision of the system [22] [29].

2.2.1 The Vacuum System

To perform simultaneous gravity gradiometry measurements, two atom clouds are needed; they are separated spatially in the experiment with the distance by which they are separated giving the baseline of the experiment; this, along with the T time between interferometry pulses, has a significant impact on the sensitivity of the device. To set this up, typically two MOTs are used, however this makes the vacuum system larger than desirable, and requires two cooling telescopes. To get around this, a single cooling re-

gion is used, designed to be in the centre of the vacuum system, as shown in figure 2.11. A scheme will be implemented in the future where the atom cloud is split into two clouds and spatially separated into the two atom interferometry regions using a moving optical lattice. To improve the sensitivity of the system, the T time between the interferometry pulses is considered. This is also limited by the size of the system, as an atom cloud can only fall so far in the short distance available. A launch configuration is used to effectively double the time that the atom cloud is in free fall, improving the sensitivity of the device.

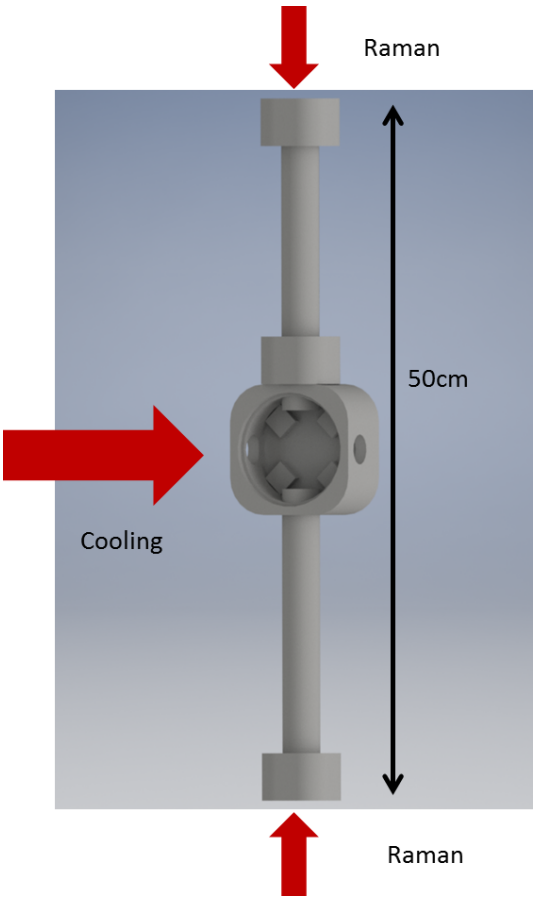


Figure 2.11: The gravity gradiometer with a split cloud scheme, showing the input beams; a single prism MOT is in the centre of the system, the atom cloud will then be split into two atom clouds and moved with an optical lattice to the two interferometer regions in a future scheme.

The vacuum system is designed to accommodate a cooling telescope attached to the MOT region, as well as either two Raman telescopes or one Raman telescope and a mirror at the top and bottom of the device; a mounting structure is designed to attach these telescopes to the vacuum chamber. Quadruple field coils are designed to fit over the prism MOT chamber, and the whole system is designed to be narrow such that the size of the magnetic shield — that is used to negate external magnetic fields to the system — is as small as possible to reduce the weight of the system. The vacuum system is built to accommodate an ion pump and a getter to maintain a low pressure in the system; a rubidium dispenser is used to generate a rubidium vapour into the chamber when a current is applied

across it; valves to open and close sections of the vacuum system; and a microwave antenna to do the microwave state preparation mentioned in section 2.1.2.2.

Each window in a vacuum system is a risk to the integrity of the system as they introduce the possibility of leaks; round windows are used to reduce this risk by avoiding high stress points. Additionally, indium seals are used to attach the windows to the vacuum system. This allows non-commercial windows to be used which reduces the cost of the system. However, compared to the alternative of copper seals, which can be heated to 400 °C, indium seals can only be heated to 120 °C [30]. When building a vacuum system, it must be heated for a prolonged time to remove gasses embedded in the chamber walls of the system and allow a sufficiently low vacuum pressure to be reached. As the system can only be heated to 100 °C due to the indium seals, the vacuum system must therefore be baked out for a longer period of time, increasing the overall time taken to build the system.

2.2.2 The Laser System

There a two main parts that make up the laser system. These are the generation of the required laser frequencies, which is achieved through the use of two IQ Modulators, devices which modulate both the in-phase (I) and quadrature (Q) inputs, allowing any arbitrary output amplitude and phase to be selected; and the system that provides the laser seed, amplification and doubling of the laser frequencies.

2.2.2.1 Frequency Generation

The IQ modulator is composed of 3 Mach-Zender interferometers, each of which contains a phase shifter, $\Phi_{1,2,3}$, and the first two containing a phase modulator, $\delta\phi_{s,c}$, shown in figure 2.12. This allows the IQ modulator to function as 3 electro-optical modulators (EOM) [31].

The phase modulators take an RF input which generates sidebands $\omega_{\pm 1}$ on either side of the input carrier frequency ω, with the separation between the carrier frequency and

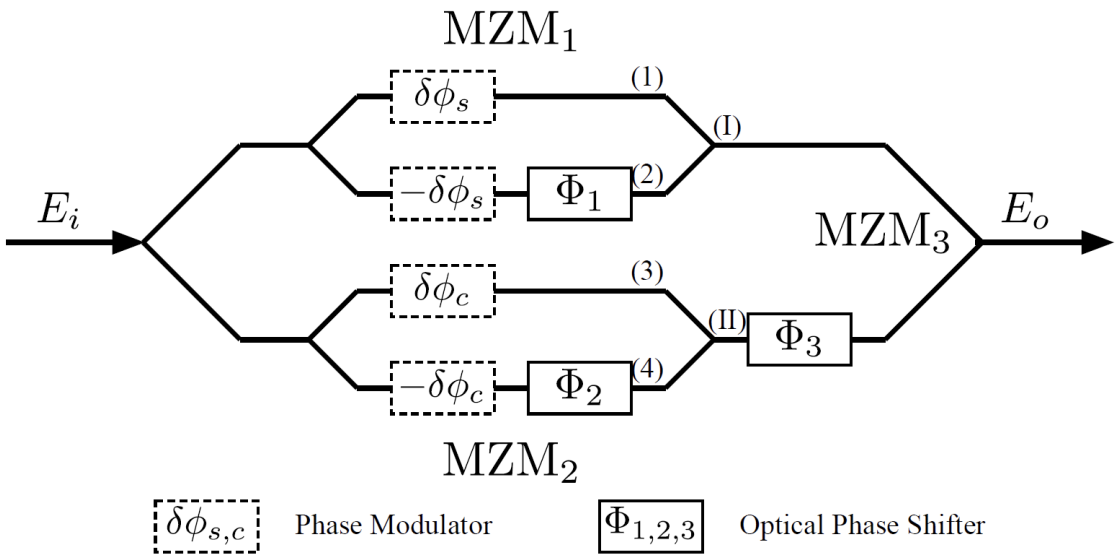


Figure 2.12: The composition of an IQ Modulator [31].

the sidebands being controlled by the input RF; meanwhile the DC signal across the phase shifters is controlled, either manually or automatically by a computer, to vary the relative strengths of the output carrier and sideband signals. From figure 2.12, Φ_1 and Φ_2 can be used to suppress the carrier signal, and Φ_3 is used to vary the ratio between the two sideband signals. This allows several different configurations of carrier and sideband frequencies, examples of which are shown in figure 2.13.

2.2.2.2 Integration into the Laser System

To perform all the steps involved in atom interferometry, many different laser frequencies are required. In a lab based system and even in the existing field systems, a large laser bench with a significant number of components is used [20] [21] [29]; this comes at a cost of size, weight, and power of the system. To make a more compact system an agile laser is used, making a system with less need for high power components by using a single laser seed to create all the required frequencies shown in figure 2.14.

The laser bench used, shown in figure 2.15, employs a few components and novel tech-

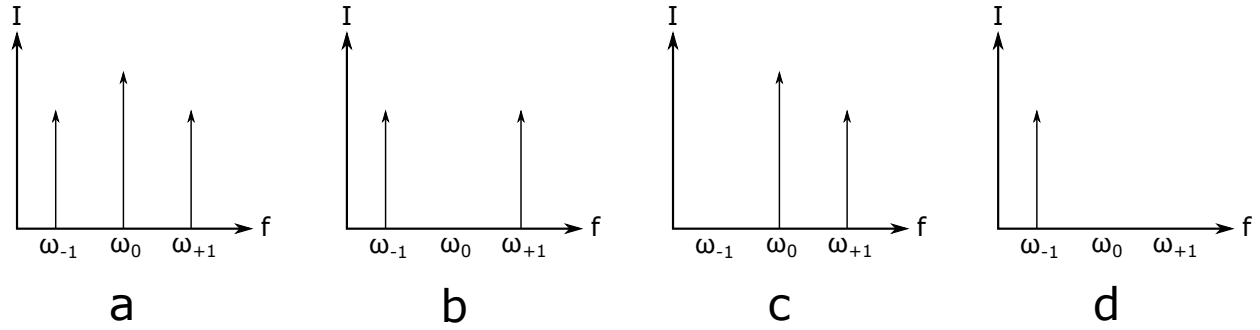
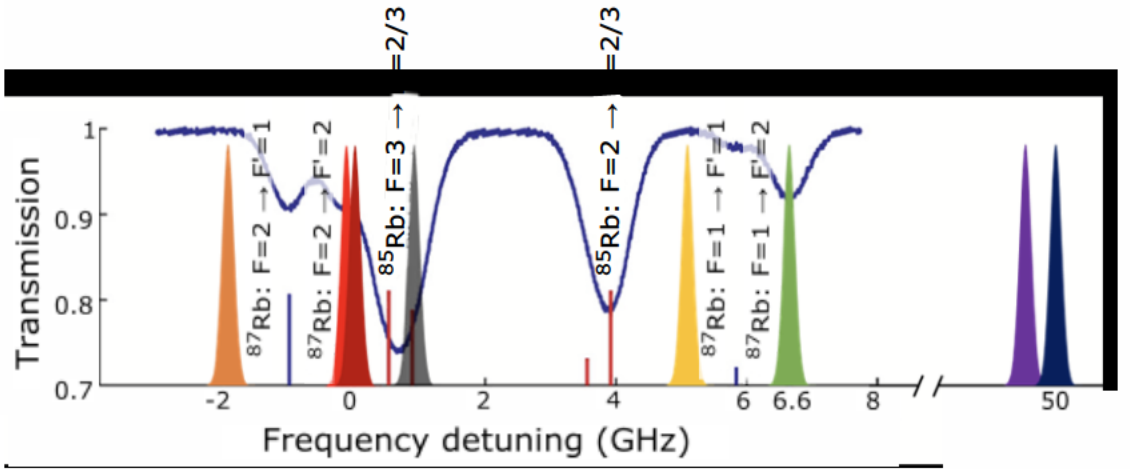
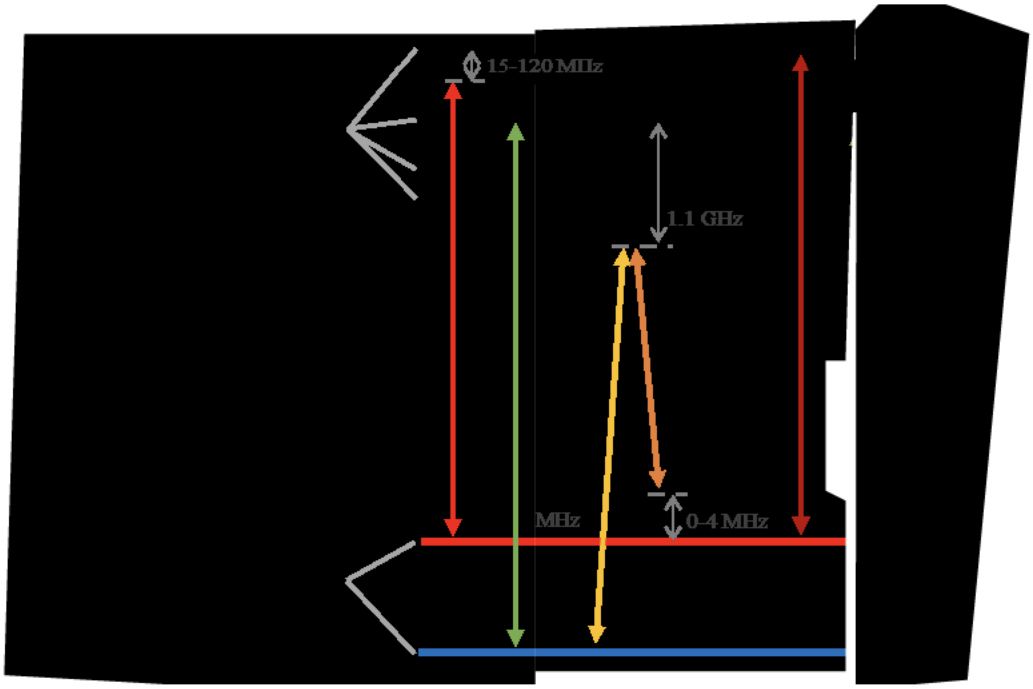


Figure 2.13: Examples of the possible sideband configurations achievable with the use of a single IQ Modulator. Of note are configurations c and d, which are used by IQ Modulator 2 and 1 respectively in figure 2.15.

niques to generate the required frequencies. A 1560 nm laser seed is used, as this is a frequency that is common in telecoms, thus both the laser seed, fibres, and other components are cheaper, more robust, and more readily available than the equivalent components at 780 nm. This laser seed is fed through a beam splitter which sends 33% of the laser power into the spectroscopy box and 67% of the laser power into the laser bench. In the spectroscopy box the frequency is doubled using the SGH (second-harmonic generator) and an EOM (electro-optic modulator) adds a modulation to the laser frequency allowing modulation transfer spectroscopy (MTS) to be performed; MTS locks the laser seed to the $|\mathrm{F} = 3\rangle \rightarrow |\mathrm{F}' = 2/3\rangle$ transition of rubidium-85 — this keeps the frequency of the laser stable, and the system can remain locked for upwards of a day under good conditions. This locking frequency is fed into two IQ modulators in series. The first IQ modulator suppresses the carrier (locking) frequency, and adds a single sideband to the signal, shown in figure 2.13d. The second IQ modulator uses this sideband as its carrier frequency, and adds a second sideband, shown in figure 2.13c. The detuning of each sideband is controlled by an RF chain, and uses frequencies shown in figure 2.14a; the result of this process is a laser signal with two discrete frequencies that can be controlled independently of each other, allowing for each pair of required frequencies to be created, shown in figure 2.14b, to be generated.



(a) The frequency detuning required to achieve all the required frequencies for the entire gradiometry sequence.



(b) The transitions used in the entire gradiometry sequence, labelled on the rubidium hyperfine structure. Cooling and repumper beams are used to cool and trap the cold atom cloud in the MOT as explained in section 2.1.1.2, two Raman beam frequencies are used for the atom interferometry sequence, explained in section 2.1.3.1, finally the detection frequency excites atoms from $|F = 2\rangle \rightarrow |F' = 3\rangle$, the atoms then de-excite to the $|F = 2\rangle$ state, emitting photons that are detected by a photodiode. This is used to find the atom number in the trap as detailed in section 2.1.1.2.

Figure 2.14: An overview of the required frequencies in the gradiometry sequence.

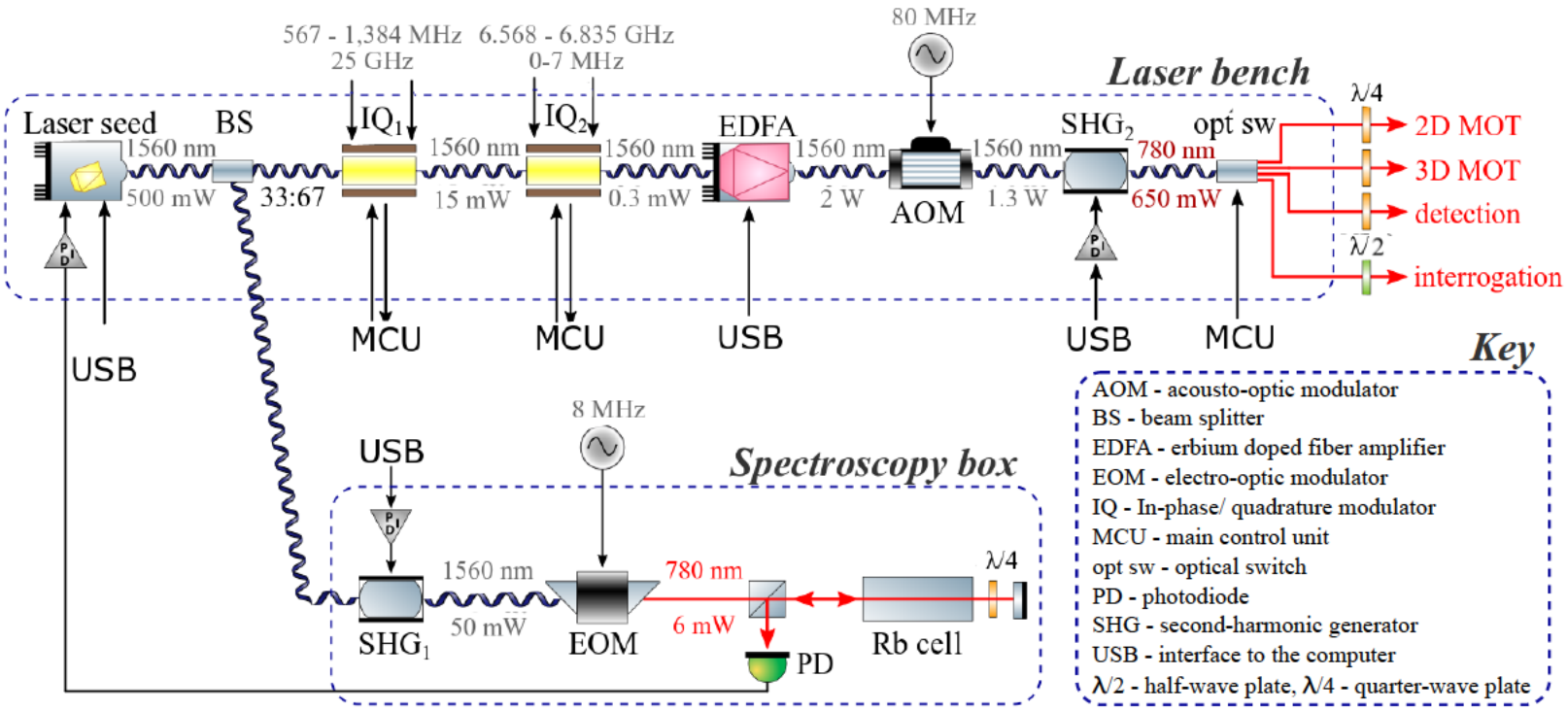


Figure 2.15: The compact laser bench used to generate the required frequencies for each stage in the atom interferometry sequence; the cooling and trapping of atoms in the MOT, the interrogation of atoms during the atom interferometry sequence, and detection. Although a 2D MOT isn't currently used in the system, we include a laser path for the 2D MOT as a possibility in the future.

The IQ modulators significantly attenuate the laser power, with only $\approx 5\%$ of the input power being transmitted across the pair. Thus, an EDFA (Erbium-doped fiber amplifier) is used to amplify the laser power. An AOM (acousto-optic modulator) is used to further shift the frequency signals by an amount larger than achievable by the IQ modulators alone and as a switch, turning the laser output on and off. Following this, the SHG (second-harmonic generator) doubles the frequency of the sideband generated by the first IQ modulator, and combines the frequencies of the sideband added by the first IQ modulator and the sideband added by the second IQ modulator, giving the required frequencies for a given stage in the gradiometry sequence. By varying the RF input into the IQ modulators and the AOM, the frequencies are changed for each stage in the sequence. Finally, the laser signal is sent through

an optical switch – this controls which telescope the laser light is sent to – and through either a quarter-wave plate ($\lambda/4$) which circularly polarises the laser beam, as required for the MOT and detection sequence, or through a half-wave plate ($\lambda/2$) which changes the orientation of the linearly polarised laser for the interrogation of the atoms during the atom interferometry sequence.

2.3 Build of the Experiment and First Results



Figure 2.16: The compact gravity gradiometer system, displayed at Cheltenham Science Festival.

For the compact gradiometer system to be constructed, each component — the vacuum system, the laser system, the relevant optics for the system — must first be constructed and assembled together. A good test that the system functions as a unit is to obtain a cold atom cloud in the MOT, as this is not possible if any part of the system is not functioning as it

should.

First, each part of the system was assembled and characterised, taking particular note of the pressure achieved in the vacuum system and the frequencies produced by the laser system. Then a cold atoms cloud was achieved in the system, with measurements taken of the atom number and loading time.

Once constructed, the complete compact system has been taken to several events to demonstrate cold atom physics; by doing this, the portability of the system is also tested. Shown in figure 2.16, the compact system is on display at Cheltenham Science Festival. The vacuum system is in a clear case for display purposes and the RF chain and laser bench are in cases to the right and left of the system respectively; when in use, these cases slot in next to vacuum system and the overall system meets the requirements discussed in section 2.2.

The system fits inside a regular hexagonal footprint with a side length of 17.8 cm. The case stands 55 cm high, making the external volume 45 l, this meets our original target of < 100 l. However the system is still operating using a bench power supply; the power supply needs to be integrated inside this volume but it is currently too large. Since leaving the project, a compact power supply has been built and is now being tested. The system weighs 17 kg and uses a power of 125 W, meeting the targets of < 20 kg and < 150 W respectively. We can improve on this by using new manufacturing techniques to allow further integration into smaller, lighter weight packages. In particular, recent work has shown 3D printed chambers that can be used to create cold atoms; these could in principle be applied to gravimetry [32].

2.3.0.1 Building the Vacuum system

The vacuum system is built, as shown in figure 2.17; a pressure of 10^{-10} mbar, as measured on the ion pump connected to the vacuum system, is reached when the system is resting, rising to a pressure of 10^{-9} mbar when the rubidium dispensers are activated to form a

cold atom cloud in the MOT. Anti-Helmholtz coils are attached to the vacuum system, and both a magnetic shield and compensation coils were attached to the frame surrounding the vacuum system. These can be used interchangeably to compensate for external magnetic fields; compensation coils are used when setting up the system as they easily allow access to the entire system and make quick adjustments possible, but they need to be adjusted manually to cancel out external magnetic fields. Meanwhile the magnetic shield is a more permanent option that doesn't require adjustments when the system is moved, at the cost of enclosing the system and making any adjustments to the vacuum system or telescopes impossible without removing the shields.

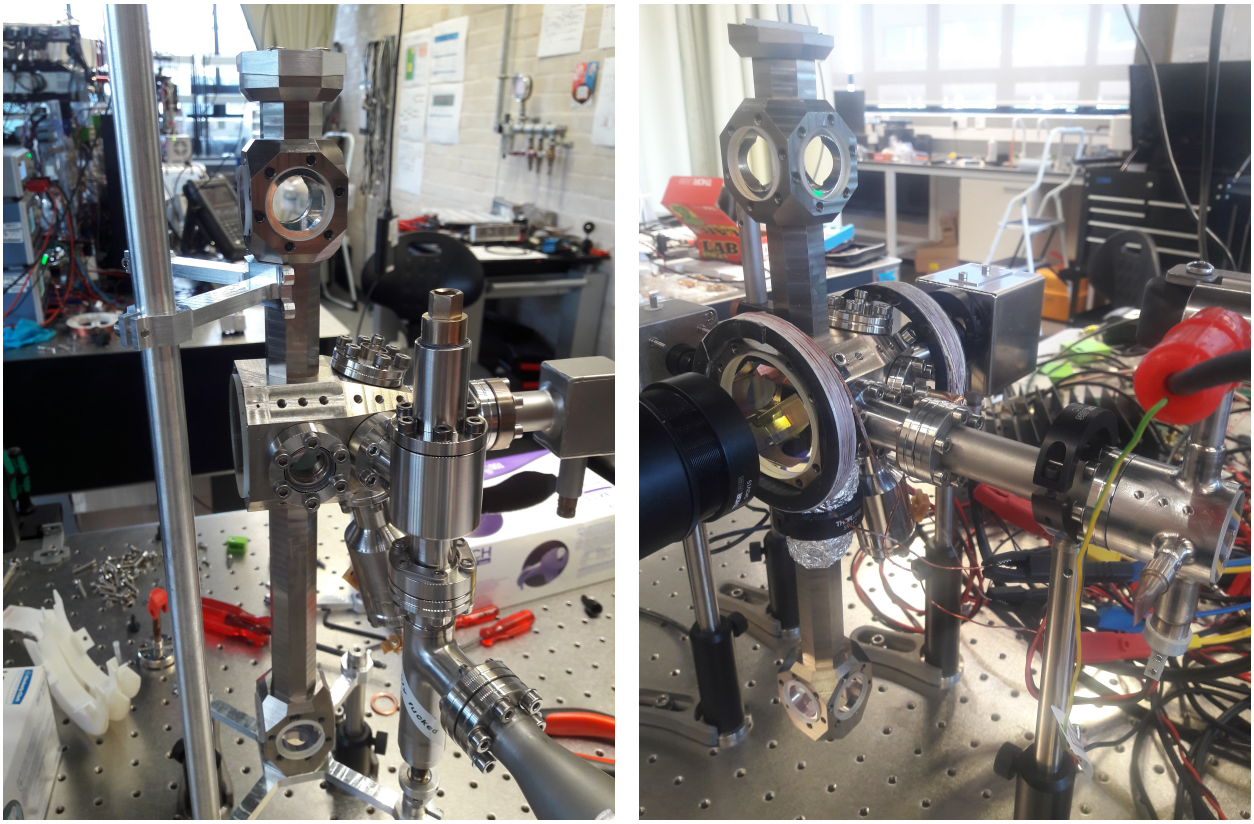


Figure 2.17: The construction of the compact vacuum system, shown both with and without the anti-Helmholtz coils and cooling telescope.

When building the vacuum system, each component is cleaned following the procedure laid out by CERN [33]. The vacuum chamber is then constructed; following this a process

of baking out the chamber is executed. This is a process of heating up the chamber when it is isolated (not connected to a pump) at atmospheric pressure; by heating the vacuum chamber, any debris that might be in the chamber will be removed, allowing for optimal pumping speed and base pressure when the vacuum pumps are turned on. The chamber is wrapped in several layers of aluminium foil to allow for even heat distribution, and is slowly heated to 130 °C at a rate of 5 °C an hour; the maximum temperature the chamber can be heated to is limited by the indium seals used in the vacuum chamber. After the baking out period, the system is cooled to room temperature and then the vacuum can be pumped to ultra high vacuum (UHV) pressure.

Once operating at UHV pressure, the vacuum chamber is also tested for leaks, with any leaks being fixed under an Argon gas atmosphere. The system is tested at each possible leak point — the indium seals around the windows, and the fastenings between different parts of the chamber — by pouring a small amount of acetone over each possible leak point and monitoring the vacuum pressure as measured on the ion pump for any variations.

2.3.0.2 Characterisation measurements of the Laser System

The IQ modulators are set up as shown in figure 2.13, to minimise the carrier frequency and create two sidebands whose frequencies can be changed independently of each other. Initially this is done manually, by individually varying the phase shifter values, Φ; a computer program is then implemented to automatically adjust these values and reach optimum noise suppression, which significantly reduces the time taken to set up the IQ modulators, from up to an hour manually, to just a few minutes with the computer programme.

The relative amplitudes of the two signals can vary, but in general V1 is increased by at least 2.24 dB compared to V2, and by 12.43 dB compared to the noise due to the unwanted carrier and sideband frequencies.

As the laser bench is constructed, the output power after each component is measured

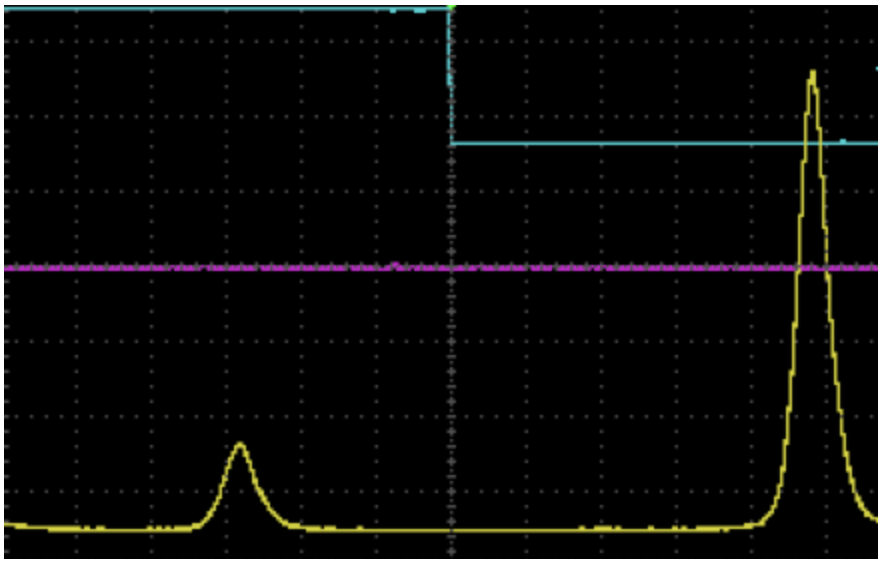


Figure 2.18: The two sidebands generated by two IQ Modulators. The sideband on the right (V1) is added by the first IQ Modulator, this is then used as the carrier frequency by the second IQ Modulator, and the sideband on the left (V2) is added.

to verify that each component is functioning correctly. Acceptable power values are noted on figure 2.15.

2.3.1 Generation of Cold Atoms in the MOT

Once each section of GI3 is constructed, the system is used to generate a cold atom cloud in the MOT at the centre of the vacuum system. This demonstrates that the system as a whole functions correctly. The trapped atoms can be seen in figure 2.20, where, as in abstract, 1.2×10^8 atoms are loaded into the MOT with a typical error of approximately 5%. The MOT has a loading time constant, τ in equation 2.2, of 0.7 s with a typical error of approximately 5%, as shown in figure 2.19. Both the atom number and the loading time of the MOT are as expected; by creating an acceptable atom cloud, the MOT in the compact vacuum system is shown to be functioning as expected, allowing the project to progress towards atom interferometry and later, gravity gradiometry.

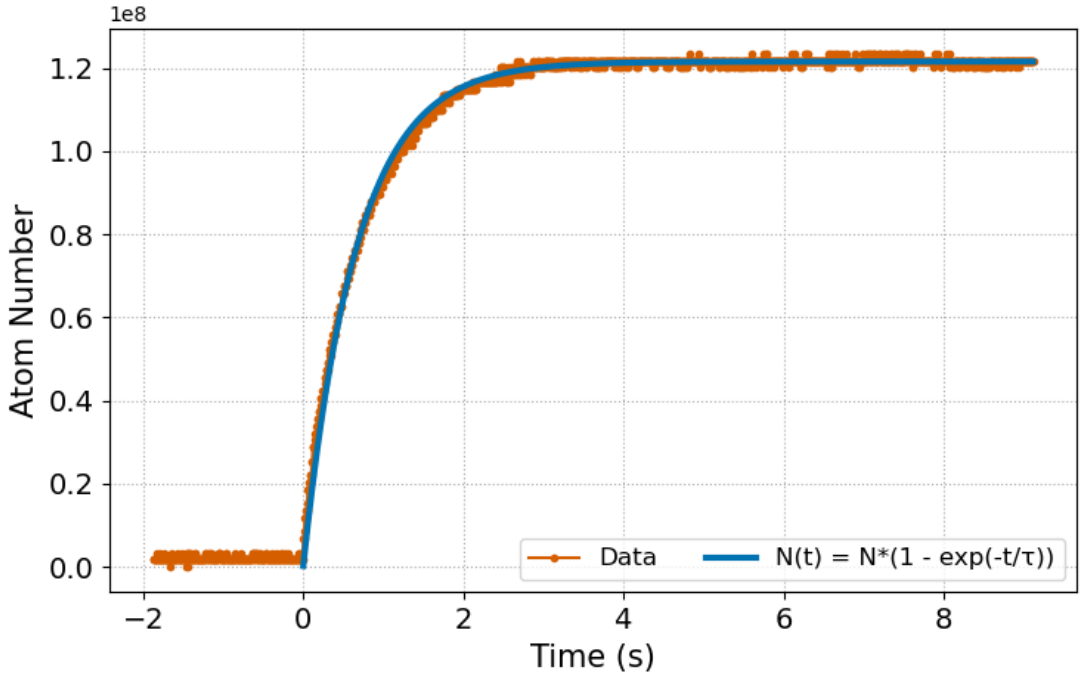


Figure 2.19: A loading curve of the increasing fluorescence from an atom cloud as it is formed in the vacuum chamber. The data is fit to equation 2.2 via non linear least squares with the error on the fit being given, as in abstract. For a single shot, the atom number is $(1.2160 \pm 0.004) \times 10^8$ and the loading time is 0.666 ± 0.002s, although the expected error for the system is at a few percent level.

2.4 System Status

When I joined the compact gravity gradiometer project, the project was still in its design phase. Over the course of this masters thesis my contributions to the project include building the vacuum system that houses the experiment, ensuring that UHV pressures of 10^{-10} mbar were reached; constructing the laser bench, utilising novel techniques to produce the required laser frequencies while still keeping a compact system; and performing the necessary characterisation measurements on the system. During my work on the project, the experiment successfully produced a cloud of 1.2×10^8 atoms, demonstrating that each part of the compact system works together as expected. Following this, I did work to investigate

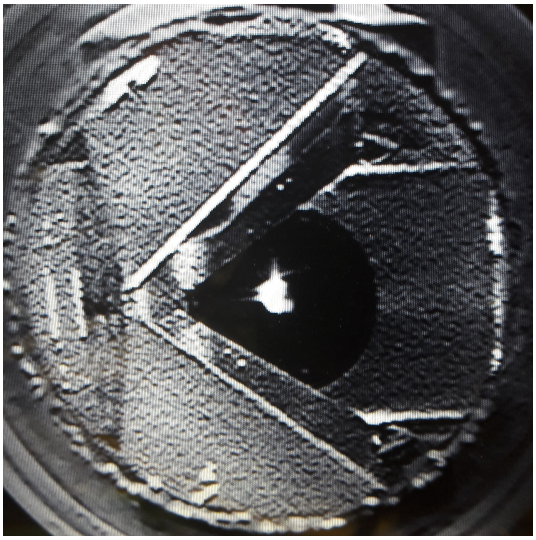


Figure 2.20: A cold atom cloud captured in the GI3 prism MOT.

the effects of background scattered light suppression on the noise of a cold atoms system.

3. The Reduction of Scattered Background Light in Cold Atom Vacuum Systems

3.1 Introduction

In many experiments, background light contributes negatively to the signal to noise ratio (SNR) and the signal to background ratio (SBR); the noise in experimental data interferes with the signal and makes the data less reliable [34].

In a cold atoms experiment, background light can contribute significantly to both the SNR and SBR. In my research, a prism MOT is used to cool and trap atoms before an atom interferometry sequence can be performed, as explained in section 2.1.1.2. In a prism MOT there are many surfaces that reflect and scatter the incident light; reducing the amount that light is scattered will significantly improve the experiment. In an atom interferometer, as noise is improved, the background noise due to scattered light becomes a limiting factor and prevents further improvements. To make a portable cold atoms system viable for use in detecting underground features, this must be taken into consideration [22][35].

To reduce scattered light, absorptive surfaces are often used — a surface appears black when its reflectance is low, where reflectance is the fraction of incident light that is reflected at a surface. Methods of blackening surfaces are examined and once characterised, an optimal black surface will be integrated into future iterations of the cold atom system explained in section 2.

There are many factors to be considered when assessing the suitability of an absorptive surface. The MOT is an ultra high vacuum (UHV) system, so a blackened coating must be UHV compatible. Additionally, the reflectance of a surface depends on the wavelength of incident light, so something that is absorptive at one wavelength of light may not be

as absorptive at other wavelengths. Finally, the relative positions of the incident light, scattering surface and detector must also be considered; a surface may have very different reflectance properties at normal incidence compared to near grazing incidence [36] All of these factors are investigated.

To reduce scattered background light in a prism MOT, a ceramic-like coating is applied to the titanium components of the vacuum chamber that houses it. The PCO35 coating is used; this is a commercially available, UHV compatible, low reflectance surface which can be applied to titanium, aluminium and magnesium alloys using a Plasma Chemical Oxidation process [23]. To test the properties of the PCO35 coating, the coating is applied to a vacuum chamber that houses a prism MOT; additionally, two identical titanium cubes are produced, one of which is coated using the PCO35 process. These cubes will be rigorously tested, both in terms of their optical properties and in their performance in a UHV system. This coating has the potential for contamination with the rubidium vapour used in a cold atoms system; in addition to testing the absorptive properties of the coated vacuum chamber, the vacuum chamber is kept at UHV for over a year to test for any signs of degradation.

3.2 Characterisation of the PCO35 coating in a vacuum

3.2.1 Theory

When operating in UHV, one of the key considerations is the gas load of the system. A higher gas load will affect the pumping speed of the vacuum, as well as the base pressure in the vacuum system [37]; this is key as a vacuum pressure of 1×10^{-8} mbar is required for atom interferometry, anything that might affect the gas load of the system and prevent the required pressure from being reached must be examined.

There are multiple factors that influence the gas load of an UHV system, these include: the initial gas load, as the vacuum system starts at atmospheric pressure and is pumped down; leaks in the system; back streaming when material from the pump travels backwards into the chamber; and outgassing. Of the factors that influence the gas load of a system, outgassing is often the most significant factor, and is difficult to eliminate [37]. When materials are at atmospheric pressure, they can absorb materials (predominantly gasses) into their surface; when these materials are in a vacuum, they outgas these materials into the vacuum chamber. As outgassing is a significant factor in the gas load of a system, for the blackened PCO35 coating to be viable for use in a cold atoms system, the outgassing rate must be low — ideally it will be the same or lower than the outgassing rate of the uncoated titanium.

From multiple literature values, the average outgassing rate for titanium is $(7.6 \pm 5.1) \times 10^{-9}$ mbar L cm^2 s^{-1} [37]. As seen by the large error on this value, the outgassing rate can vary significantly, and multiple factors influence this, including variation in the manufacturing process; the method used to measure the outgassing rate; the local atmospheric pressure; and so on. To determine if the PCO35 will be suitable for use in an UHV and to allow for meaningful comparison between the coated and uncoated titanium, all of these effects are being kept constant across our measurements; aside from the application of the PCO35 coating the two test blocks are being treated identically. It is also useful to know the exact make-up of the outgassed materials, which is determined with an residual gas analysis.

3.2.2 The Test Vacuum System

A vacuum test chamber is made to investigate the behaviour of an uncoated titanium cube, a blackened titanium cube with the PCO35 coating and the empty vacuum test chamber as shown in 3.3. Before measurements are taken, both the samples and the test chamber must be cleaned. The sample cubes are rigorously cleaned in the same way vacuum components

are cleaned before they are assembled. This is done following a procedure laid out by CERN [33] as detailed in section 2.3.0.1.

Following this, a process of baking out the chamber is executed as described in section 2.3.0.1; with the system being slowly heated to a temperature of 130 °C. This is limited by the indium seals used on the windows of the vacuum chamber, the PCO35 coating alone can be heated up to a temperature of 150 °C [23]. This procedure must be repeated every time the vacuum test chamber is opened to change the sample, before any outgassing measurements can be taken. This work has been published in API Advances, under the title "Reduction of background scattered light in vacuum systems for cold atoms experiments" [22]. The authors contributions were executing the experimental measurements and analysing the data.

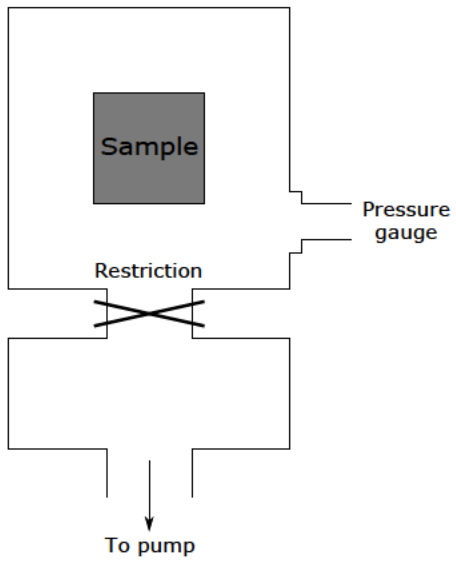


Figure 3.1: A test vacuum system to measure the pressure rate-of-rise as a sample outgasses.

There are several different methods that can be used to measure the outgassing rate in a vacuum system, including throughput, conductance modulation and rate of rise; independent of the method used, measurement can only be started if the vacuum pressure is below 1×10^{-2} mbar [37]. The rate of rise method is used in the test vacuum system — this is one of the more simple methods for measuring outgassing; a sample is placed in a vacuum chamber which is then pumped down and isolated by closing a valve as shown in figure 3.1. As the sample outgasses, the pressure in the isolated chamber increases; the outgassing rate of a sample is calculated by using $q = \frac{dP}{dt} \times \frac{V}{A} \approx \frac{\Delta P}{\Delta t} * \frac{V}{A}$ for a vacuum chamber of volume V and a sample with surface area A.

The approximation is valid when measuring an increase in pressure, ΔP, over a short

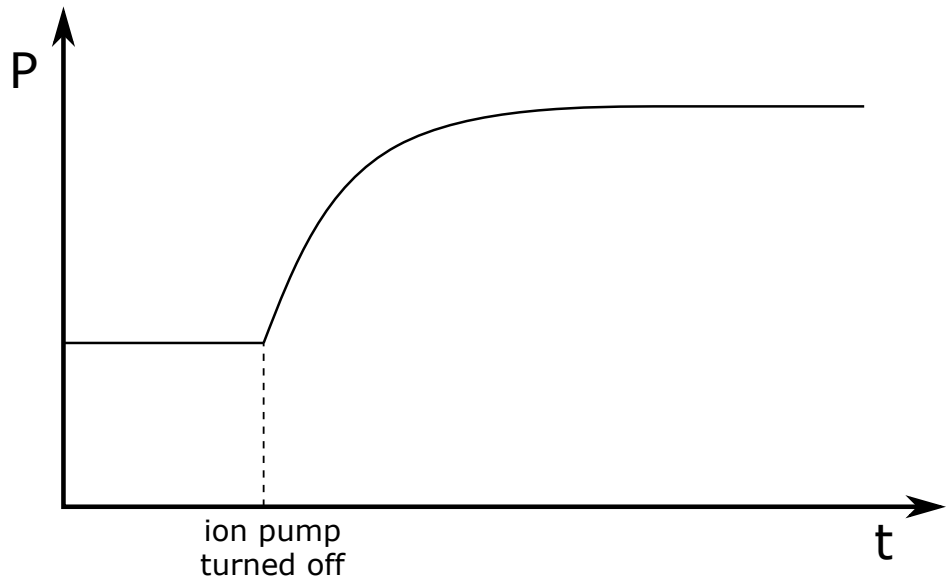


Figure 3.2: The expected variation of pressure over time inside a vacuum chamber that is isolated, when performing rate of rise measurements.

time period, Δt and should be measured a short time after the vacuum chamber is isolated and the rate of rise is approximately linear. The pressure in the system should behave as in 3.2.

In the vacuum test chamber a turbo pump and an ion pump are used. To perform rate-of-rise measurements, the valve to the turbo pump is closed and the turbo pump is turned off. Subsequently, the valve to the ion pump is closed and the ion pump is turned off — at this point the rate-of-rise measurements start, and the pressure is measured for at least 10 hours. The ion pump is then turned back on and the pressure is once again measured and monitored for at least 10 hours. A Pfeiffer Residual Gas Analyser (RGA) is also connected to the test vacuum system, this is used to perform a Faraday MCD analysis and allows for both qualitative and quantitative analysis of the composition of the gases in the vacuum test chamber. When the RGA is turned on the pressure in the vacuum rises from 2×10^{-9} mbar to 3.5×10^{-8} mbar; this is typical behaviour for hot-filament vacuum gauges [38]. The read

out from the RGA is given in ion current, by measuring the pressure in the chamber when RGA measurements are taken, this is converted to concentration.

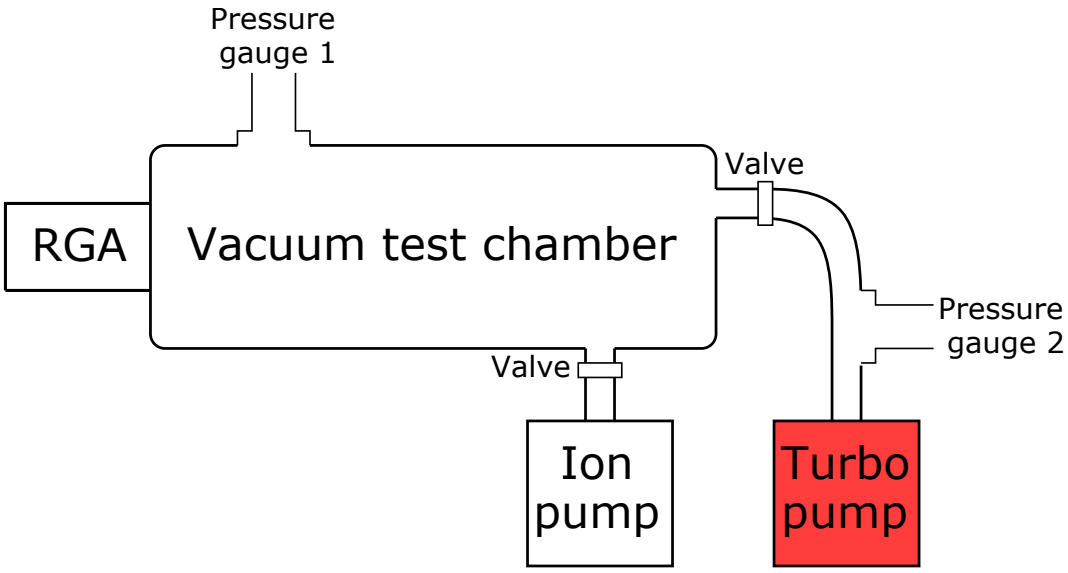


Figure 3.3: The vacuum test chamber used to direct compare the performance of uncoated Titanium, a material typically used in a vacuum chamber, and blackened titanium with a PCO35 coating. The test chamber is used to measure the outgassing of the two samples, as well as perform a qualitative and quantitative analysis of the gases in the vacuum chamber.

3.2.3 Measurements

Measurements are taken of the outgassing rate of the empty vacuum chamber, the vacuum chamber with the uncoated titanium cube, and the vacuum chamber with the PCO35 coated titanium cube, as shown in figure 3.4. From the outgassing rate of rise curves, the outgassing rates for the three systems are calculated. The outgassing rates for the empty chamber, coated and uncoated cubes are $q = 2.26 \times 10^{-8}$, $q = 7.08 \times 10^{-8}$ and $q = 7.06 \times 10^{-8}$ mbar L cm^2 s^{-1} respectively. These are significantly small, suggesting that the outgassing rate increase due to the PCO35 coating is less than is resolvable by the system.

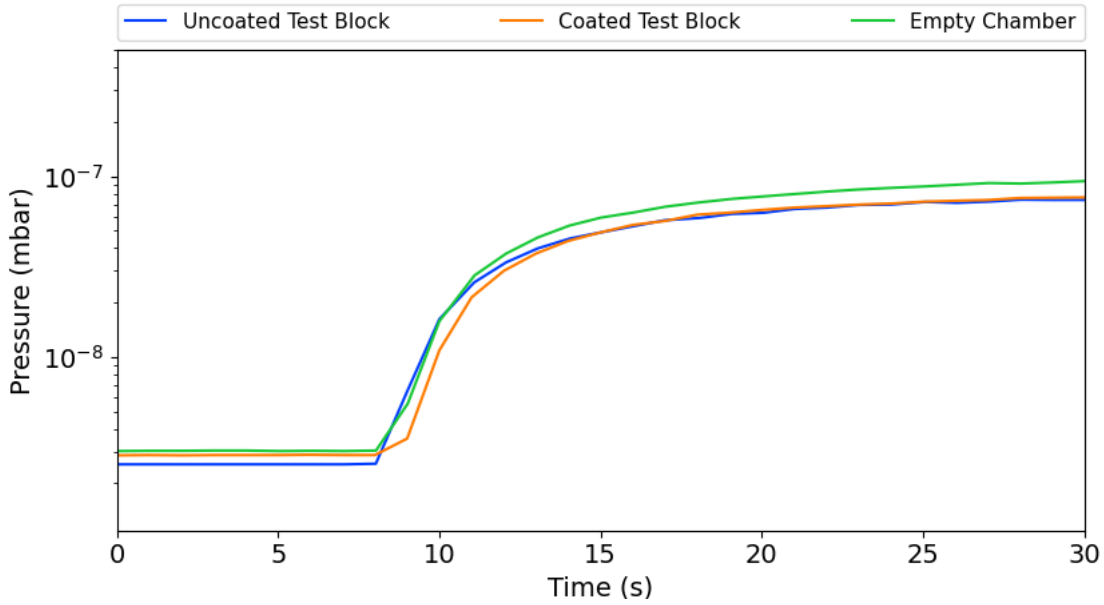


Figure 3.4: Outgassing rate of rise measurements comparing the empty test chamber, and the test chamber containing the uncoated and coated titanium samples. The difference in the outgassing rate of rise is not resolvable by the system, thus any contribution by the PCO35 coating is negligible for this vacuum system.

The properties of the residual gasses introduced by the PCO35 coating are measured using a residual gas analysis, shown in figure 3.5. The composition and amount of residual gasses in the empty test chamber, and the test chamber with the coated cube are very similar; this suggests that the PCO35 coating doesn't introduce a sharp increase in any element in the vacuum test chamber over the range examined.

The outgassing rate and RGA measurements show that the PCO35 coating is suitable for use in an UHV environment.

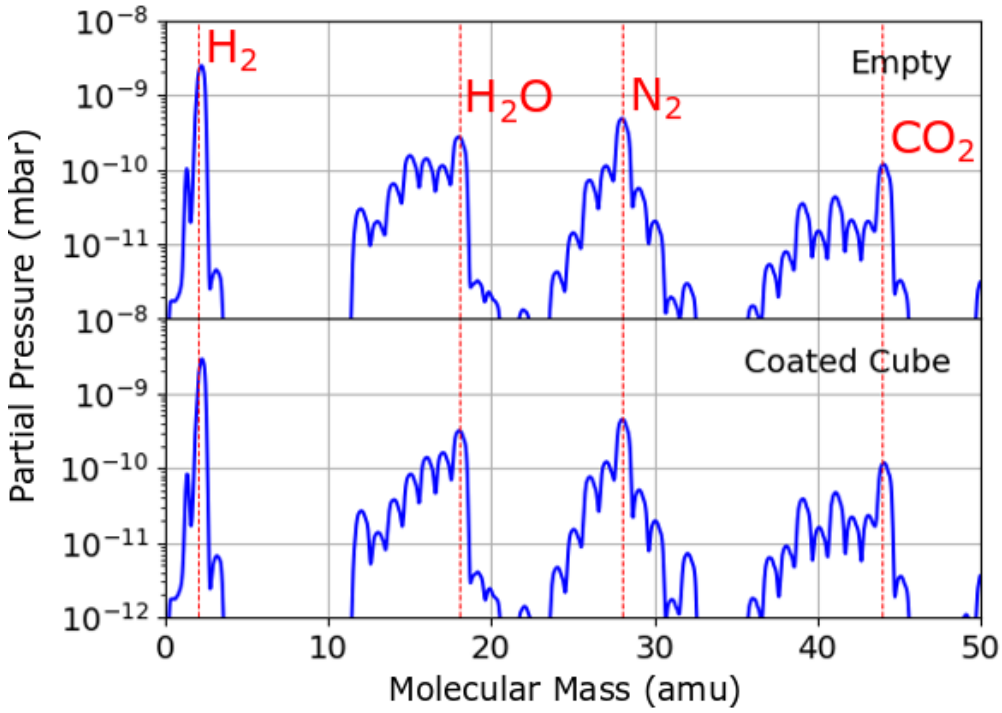


Figure 3.5: Residual gas analysis of the empty vacuum test chamber and the test chamber containing the coated titanium cube. Measurements are taken 24 hours after cleaning and bakeout of the vacuum chamber; the two measurements show no change in excess water or complex hydrocarbons across the measured range [22].

3.3 Characterisation of optical properties

3.3.1 Theory

To determine how "black" a surface is, its reflectance is measured. Reflectance is defined as the ratio of incident light to the reflected light by a surface. Optical reflectance is typically determined by the bidirectional reflectance distribution function (BRDF), which takes into account the relative angles of the incident light, the reflecting surface, and the reflected light [36]. The BRDF is defined as

$$f_r(\theta_i, \theta_r, \phi_r) = \frac{P_r D^2}{P_i A cos(\theta_r)} \tag{3.1}$$

where P_r is the power reflected to a detector from incident power P_i, with a detector of area A and distance D from the reflecting surface. θ_i and θ_r are the incident and reflected polar angles respectively, and ϕ_r is the reflected azimuthal angle, as defined in figure 3.6.

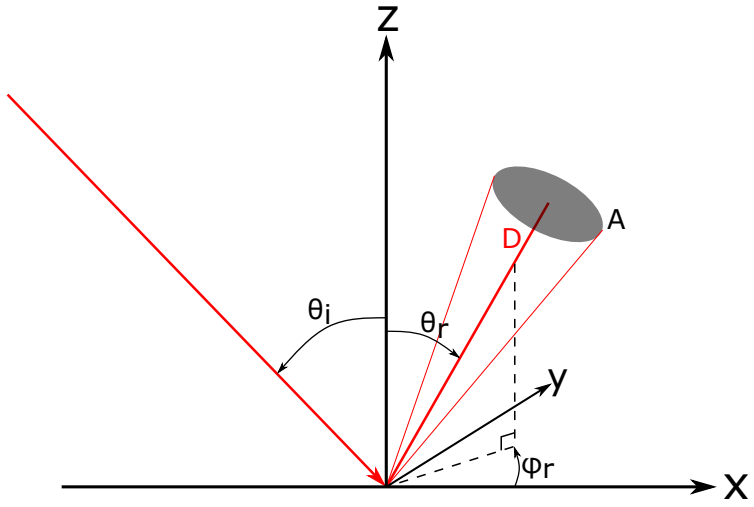


Figure 3.6: Theoretical set-up to measure the BRDF of a surface in the x-y plane.

It is also useful to use the BRDF of a surface in comparison to an ideal Lambertian surface;

Lambertian reflectance is the property that defines an ideal "matte" surface, which has diffuse reflectivity. The apparant brightness of a Lambertian surface is constant regardless of the angle of observation, giving a constant BRDF value [39]. For a black surface that won't contribute to scattered background light, ideal reflectance would be approaching that of a Lambertian surface.

3.3.2 Experimental Set-Up

The BRDF of both an un-coated titanium cube and a blackened titanium cube is measured. To properly measure the BRDF of a substance, measurements need to be taken over a range of both incident and reflective angles. The sample cubes are placed at the centre of a turntable, with a detector photodiode that can be rotated independently around the axis of rotation of the turntable, positioned attached to be rotatable around the sample, as shown in figure 3.7. A laser beam with beam waist $1/e^2 = 0.37$ mm is positioned so that the laser beam intersects the axis of rotation; this beam is split using a 50:50 beam splitter — half of the laser power being directed to a monitor photodiode to check for and record any fluctuations in the incident laser power.

Measurements of the BRDF are taken for angles of $\theta_i = 0°$ over a range of $\theta_r = -80° \rightarrow +80°$, and $\theta_i = 55°$ over a range of $\theta_r = -40° \rightarrow +85$. For the measurements where $\theta_i = 0°$, no measurements are taken for $\theta_r = -20° \rightarrow +20°$, as the detector photodiode blocks the incident light in this position. Measurements are taken using the range of wavelengths that are available to us: $\lambda = 462$ nm, 679 nm, 780 nm, 813 nm and 1560 nm. A full characterisation of the behaviour of the PCO35 coating is valuable; but of particular interest is $\lambda = 780$ nm, as this is the wavelength used in a rubidium MOT chamber.

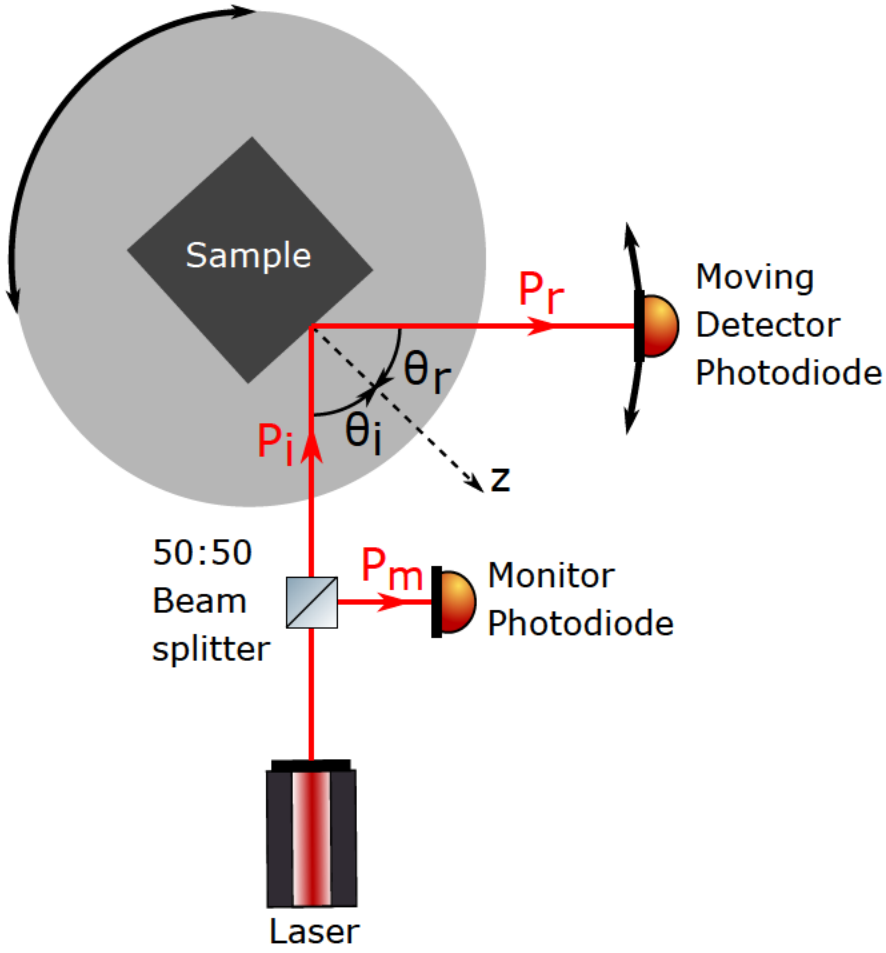
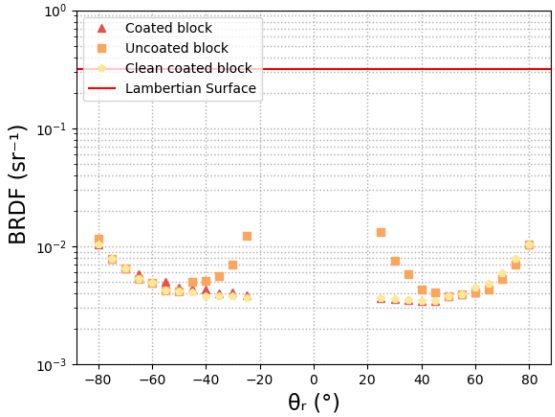


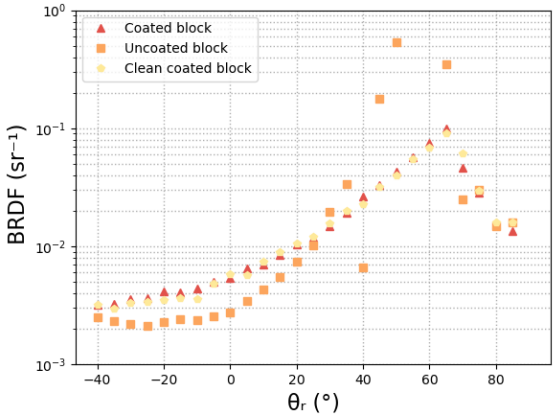
Figure 3.7: Experimental set-up to measure the BRDF of uncoated and coated Titanium cubes, labelled sample.

3.3.3 Measurements

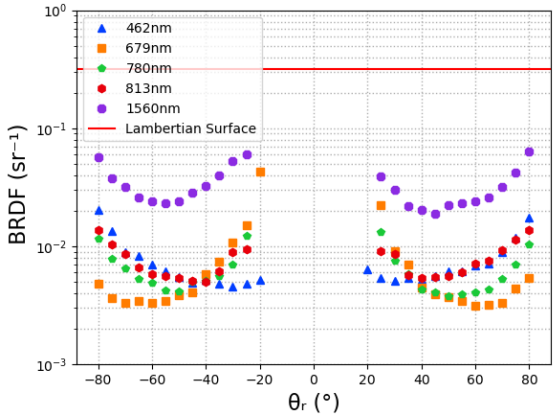
The performance of the PCO35 coating is thoroughly tested, shown in figure 3.8; it proves to reduce the amount of scattered light compared to the uncoated titanium across all the conditions tested. It is clear that the BRDF varies significantly with the wavelength of incident light, with the coated block giving a lower BRDF — therefore a reduction in scattered light — across all the wavelengths tested, proving that the PCO35 coating is suitable for a range of applications. The biggest variation in the total scattered light from the blocks



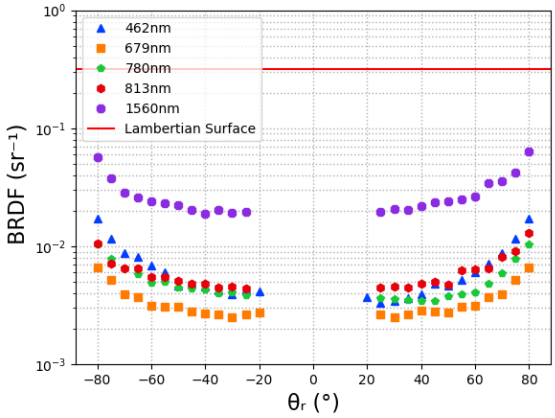
(a) Coated and uncoated titanium with $\lambda = 780$ nm at $\theta_i = 0°$ incidence.



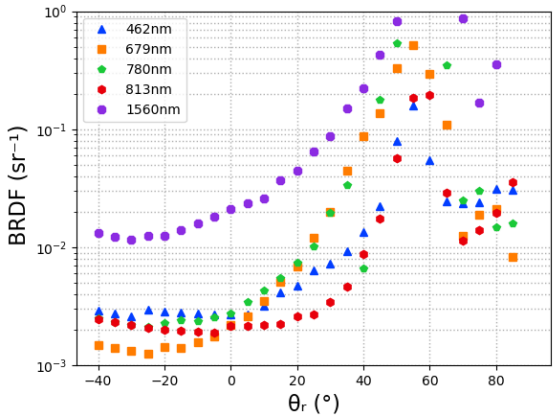
(b) Coated and uncoated titanium with $\lambda = 780$ nm at $\theta_i = 55°$ incidence.



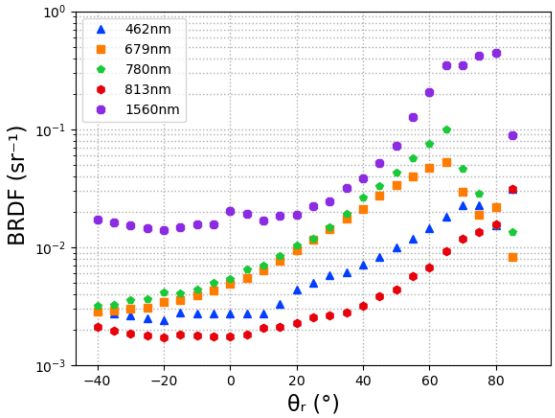
(c) Uncoated titanium at $\theta_i = 0°$ incidence.



(d) Coated titanium at $\theta_i = 0°$ incidence.



(e) Uncoated titanium at $\theta_i = 55°$ incidence.



(f) Coated titanium at $\theta_i = 55°$ incidence.

Figure 3.8: A comparison of the BRDF properties of coated and uncoated titanium, across a range of wavelengths (462 nm, 679 nm, 780 nm, 813 nm, 1560 nm) and two incident angles of light ($\theta_i = 0°, 55°$).

occurs at 780 nm, which corresponds to the wavelength of most interest in this experiment, as it is used to cool rubidium atoms in the MOT chamber; the smallest variation in the total scattered light occurs at 462 nm. When light at 55° incidence is used, shown in subfigures 3.8e, 3.8f, it can be seen that as well as being reduced for the coated block, the BRDF profile also broadens, which is as expected [22].

3.4 The use of the PCO35 coating in a Cold Atom Vacuum System

3.4.1 Construction of the test chamber

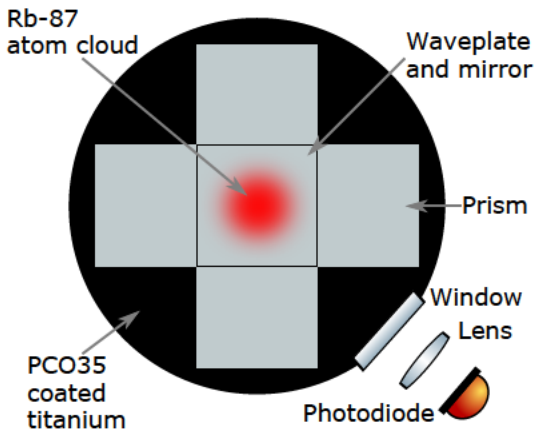
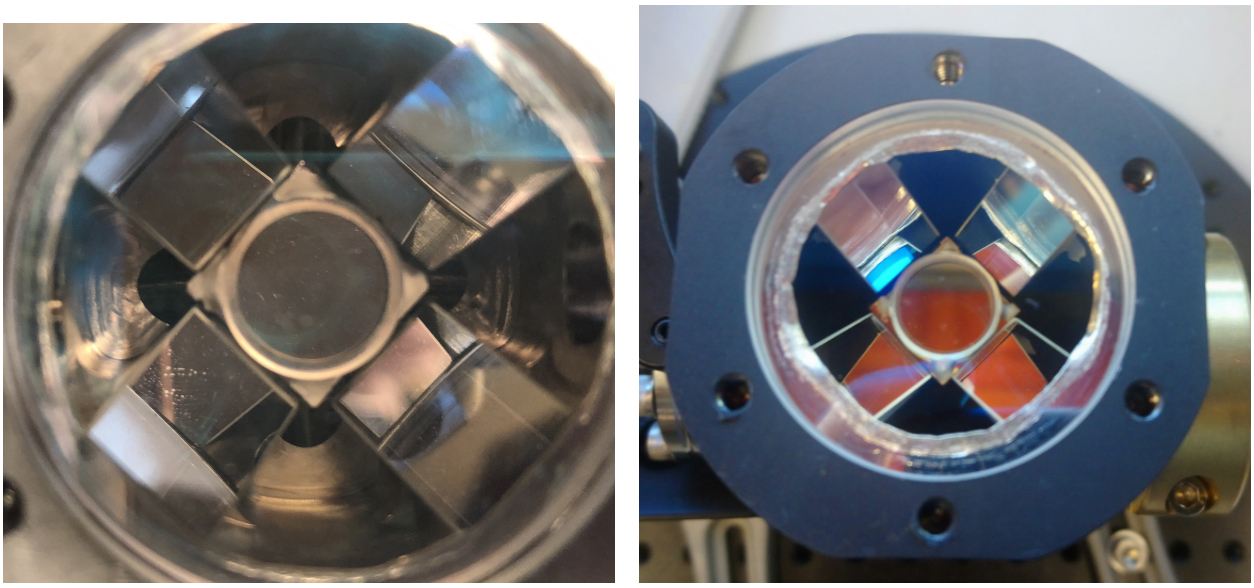


Figure 3.9: A diagram of the a prism MOT with a PCO35 coating. A window and lens are used to measure both the light incident on a photodiode by a fluorescing atom cloud, and the background light in the chamber when there is no atom cloud present.

Cold atoms systems use primarily reactive elements, so the PCO35 coating must be tested in these conditions to ensure compatibility. In the atom interferometry system discussed in section 2.2, rubidium (Rb-87) is used. A prism MOT chamber is constructed using titanium blackened with the PCO35 coating to make the vacuum chamber shown in figure 3.9; this is made to match an already constructed prism MOT system made with uncoated titanium as laid out in [40]. Both uncoated and coated vacuum chambers are shown in figure 3.10

The PCO35 coating was applied to the titanium before the vacuum chamber was constructed; the vacuum chamber components were cleaned using the method explained in



(a) A demo prism MOT, made with uncoated titanium.

(b) A prism MOT with the PCO35 coated titanium chamber.

Figure 3.10: The two prism MOT systems used to test the capabilities of the PCO35 coating in a cold atoms system

section 3.2.2 and the vacuum system was baked out at a temperature of 100 °C for 72 hours, then it was pumped down pressure of 10^{-9} mbar which is maintained with a 2 l s^{-1} ion pump.

Both the coated and uncoated prism MOTs use a fibre laser system, explained in section 2.2.2, to deliver a beam of beam waist $1/e^2 = 30$ mm and power, $P = 14.6$ mW to the chamber. The atom cloud is formed in the chamber, and its fluorescence is measured using the photodiode in figure 3.9.

3.4.2 Comparison between a coated and uncoated test chamber when producing a cold atom cloud

When atoms are loaded into the two prism MOT systems to identify the effect, if any, of the PCO35 coating on the cold atoms system. In the uncoated prism MOT, seen in figure 3.10a,

$(4 \pm 0.6) \times 10^7$ atoms are loaded into the chamber with a loading time of 0.9 s and a typical error of a few percent, at a measured pressure of 8.6×10^{-7} mbar, obtained from the ion pump current which may include some leakage current; in comparison, the blackened prism MOT, seen in figure 3.10b, loads $(6 \pm 0.9) \times 10^7$ atoms at a pressure of 9.5×10^{-7} mbar as obtained from the ion pump current, with a loading time of 1.30 s and a typical error of a few percent [22]. By measuring the scattered light from the MOT, and the scattered light contribution from the chamber and any background fluorescence of the atoms, it was found that the coated test chamber reduced the background light by $40\% \pm 4\%$.

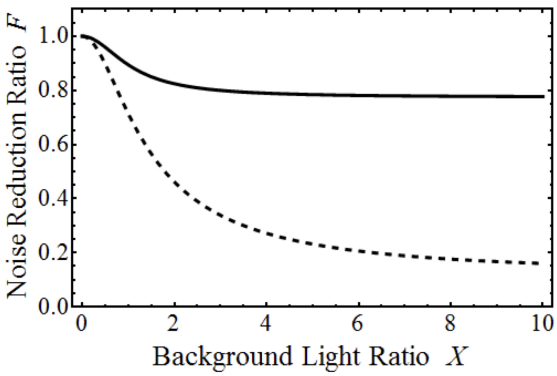


Figure 3.11: The amount by which the noise reduction ratio, F, is reduced by a reduction in background light, where X is the ratio between the noise from background light compared to the noise from other sources. The solid line shows a reduction in background light by $Y = 0.6$; the dashed line shows a reduction by $Y = 0.016$.

Comparing the two systems, there is no measurable negative effect introduced by the blackened coating on the atom number or the loading time. Furthermore, since its construction, the coated vacuum chamber has operated in a vacuum for two years, showing long term capabilities.

In a system, noise can be split into two variables: noise due to background light, σ_b, and noise from all other noise sources, σ_1. The overall noise is therefore $\sigma_2 = \sqrt{\sigma_1^2 + \sigma_b^2}$, and the aim in an experiment is to reduce this overall noise. If a blackened coating affects the background light by a factor Y, where Y = 1 gives no reduction in background light and Y = 0 gives a total reduction in background light, the

total noise will be reduced by a factor F given by [22]

$$F = \sqrt{\frac{1 + YX^2}{1 + X^2}} \tag{3.2}$$

$$X = \frac{\sigma_b}{\sigma_1}. \tag{3.3}$$

Two cases for the reduction in optical power of the background light are chosen, Y= 0.60 and Y= 0.016, corresponding to the reduction in the background light measured in coated test chamber set up in section 3.4.1, and to the values measured from figure 3.8 respectively.

From equation 3.3 it can be seen that in the limit of X $\rightarrow$ 0 there is no reduction in F as $\sigma_1 \gg \sigma_b$ and background light is an insignificant noise source. In the limit of high X, the reduction in noise is equal to the square root of the reduction in background light, Y [22]. Choosing Y = 0.60, using the reduction in background light in the coated test chamber compared to the uncoated test chamber, F $\rightarrow \sqrt{\text{Y}} = 0.77$ in the limit of high X, giving a noise reduction of 0.23 or 23%.

This can be seen in figure 3.11, where the function F is plotted against the background light ratio, X. Using Y = 0.60, shown by the solid line in figure 3.11, it is found that as X increases, the noise reduction ratio approaches F = 0.77; again this gives a possible noise reduction of 0.23 or 23% for a generalised cold atos system using a prism MOT. This gives a significant improvement in a cold atoms system with small increase in complexity and will be included in future cold atoms systems that are built. Equation 3.3 allows for generalisation to any vacuum system using the PCO35 coating given that the background light level is known.

4. Conclusion

Cold atoms based gravity sensors have exciting applications for use in field surveys; to be competitive in the field of commercial gravity sensors, a compact system is required such that the device can be moved and operated by a single person. A compact cold atoms system was built, taking into account size, weight and power constraints of < 10 l, < 20 kg and < 150 W respectively. An ultra-high vacuum system was built to achieve a pressure of 10^{-10} mbar as measured by the ion pump connected to the system; the vacuum system houses a prism magneto optical trap that cools and traps a cloud of rubidium atoms, with the system designed such that this atom cloud can be either dropped or split and launched to facilitate a gravimetry or gradiometry atom interferometry sequence respectively, with future work needed to achieve this. A compact laser system was built using novel techniques; combining two IQ Modulators to make a system that produces the required range of laser frequencies for an entire atom interferometry sequence, as shown in figure 2.14, using a single laser seed. The compact system is used to create a cold atom cloud, trapping 1.2×10^8 atoms in the MOT, with a loading time of 0.7 s, the expected error for the system is at the few percent level. This demonstrates that every part of the compact system is working correctly for the generation of a cold atom cloud with work needed to make the system into an atom interferometer.

In a cold atoms based atom interferometer, background light forms a significant negative contribution to the signal to noise (SNR) and signal to background (SBR) ratios. An absorptive coating is investigated to reduce the amount of background light in the system. A ceramic-like PCO35 coating is applied to titanium using a plasma chemical oxidation process. This is tested both to determine the absorptive qualities of the coating and to determine the suitability of the coating in a UHV environment. The reflectance of the PCO35 surface is measured across a range of incident angles and incident wavelengths, this is compared to

the reflectance of an uncoated titanium surface. The bidirectional reflectance distribution function is calculated for these measurements and the PCO35 coating is proven to reduce the amount of scattered light across all investigated wavelengths and angles. The biggest decrease in scattered light between the coated and uncoated blocks is observed at 780 nm, which corresponds to the wavelength of light that is used to cool rubidium atoms in a MOT and is therefore of particular interest in this experiment.

The PCO35 coating is tested in a test vacuum system, and no significant outgassing is observed. The PCO35 coating is then applied to the interior of a MOT chamber; this chamber is used to form a cloud of rubidium atoms, this is compared to results in an uncoated but otherwise identical test MOT chamber. The uncoated prism MOT traps $(4 \pm 0.6) \times 10^7$ atoms with a loading time of 0.9 s and a typical error at the few percent level, while the coated prism MOT traps $(6 \pm 0.9) \times 10^7$ atoms with a loading time of 1.3 s and a typical error at the few percent level — no significant difference is observed. For a generalised cold atoms system using a prism MOT, the blackened coating gives a possible noise reduction of 23%. This is a significant improvement, and in future iterations of building a compact atom interferometer, an absorptive coating should be applied to the vacuum chamber.

Acknowledgements

My supervisors Dr Michael Holynski, Prof Kai Bongs and Dr Mehdi Langlois have been instrumental throughout this project, in particular I would like to thank Mike for his constant support both with this project and with many (many) pastoral meetings. I worked closely with Mehdi and Dr Luuk Earl, a PhD student, throughout this project. Your scientific ability and drive inspired me throughout this project, and it was an absolute pleasure to work with you both.

I would like to thank Dr Jamie Vovrosh first for working with me in researching the PCO35 absorptive coating, and for pushing through the paper on this research [22]; I also want to thank him for his support during my undergraduate final year project — he and Mike welcomed me to the research group with warmth. I would also like to thank the whole Cold Atoms group at the University of Birmingham, in particular those within the Quantum Technology Hub of Sensors and Timing, it has been a pleasure to work alongside each and every one of you.

Finally, to my parents, your love and support has been a constant positive force throughout my life and I cannot thank you enough. To Josie, thank you for your unwavering love, even (especially) when I was tired and stressed. Your support and constant belief in me helped me push through poor mental health (and a worldwide pandemic) and come out the other side with work that I'm proud of.

Bibliography

[1] Kasevich M, Chu S. Measurement of the gravitational acceleration of an atom with a light-pulse atom interferometer. Appl Phys B Photo. 1992;54:321.

[2] Kasevich M, Chu S. Atomic interferometry using stimulated Raman transitions. Phys Rev Lett. 1991;67:181.

[3] Foot C. Atomic Physics. OUP Oxford; 2005.

[4] Abend S, Gersemann M, Schubert C, Schlippert D, Rasel EM, Zimmermann M, et al. Atom interferometry and its applications. arXiv;2001.10976.

[5] Rosi G, Sorrentino F, Cacciapuoti L, Prevedelli M, Tino GM. Precision measurement of the Newtonian gravitational constant using cold atoms. Nature. 2014;510:518521.

[6] Parker RH, Yu C, Zhong W, Estey B, Mller H. Measurement of the fine-structure constant as a test of the Standard Model. Science. 2018;360:191.

[7] Schlippert D, Albers H, Richardson LL, Nath D, Heine H, Meiners C, et al. Ground Tests of Einstein's Equivalence Principle: From Lab-based to 10-m Atomic Fountains. arXiv;1507. 05820.

[8] Bonnin A, Zahzam N, Bidel Y, Bresson A. Characterization of a simultaneous dual-species atom interferometer for a quantum test of the weak equivalence principle. Phys Rev A. 2015;92:023626.

[9] Graham PW, Hogan JM, Kasevich MA, Rajendran S. New Method for Gravitational Wave Detection with Atomic Sensors. Phys Rev Lett. 2013;110:171102.

[10] Wu S, Su E, Prentiss M. Demonstration of an Area-Enclosing Guided-Atom Interferometer for Rotation Sensing. Phys Rev Lett. 2007;99:173201.

[11] Peters A, Chung KY, Chu S. Measurement of gravitational acceleration by dropping atoms. Nature. 1999;400:849.

[12] Dickerson SM, Hogan JM, Sugarbaker A, Johnson DMS, Kasevich MA. Multiaxis Inertial Sensing with Long-Time Point Source Atom Interferometry. Phys Rev Lett. 2013;111:083001.

[13] McGuirk JM, Foster GT, Fixler JB, Snadden MJ, Kasevich MA. Sensitive absolute-gravity gradiometry using atom interferometry. Phys Rev A. 2002;65:033608.

[14] aosense; 2019. Available from: `https://aosense.com/`.

[15] Precision Quantum Sensors; 2019. Available from: `https://www.muquans.com/`.

[16] Hinton A, Perea-Ortiz M, Winch J, Briggs J, Freer S, Moustoukas D, et al. A portable magneto-optical trap with prospects for atom interferometry in civil engineering. Phil Trans R Soc A;375.

[17] Studies of industrial gravity measurement applications.;. Available from: `http://www.rsksigma.co.uk/`.

[18] Gravity sensors; 2020. Available from: `https://scintrexltd.com/applications/gravity/`.

[19] Bongs K, Holynski M, Vovrosh J, Bouyer P, Condon G, Rasel E, et al. Taking atom interferometric quantum sensors from the laboratory to real-world applications. Nature Rev Phys. 2019;1:731.

[20] Schmidt M. A mobile high-precision gravimeter based on atom interferometry. Humboldt-Universitt zu Berlin; 1978.

[21] Rammeloo C. Optimisation of a Compact Cold-Atoms Interferometer for Gravimetry. University of Birmingham; 2018.

[22] Vovrosh J, Earl L, Thomas H, Winch J, Stray B, Ridley K, et al. Reduction of background scattered light in vacuum systems for cold atoms experiments. AIP Advances. 2020;10.

[23] Instruments: Sura Instruments;. Available from: http://www.sura-instruments.de/en/.

[24] Holynski M. Creating a two dimensional cold mixture experiment. University of Birmingham; 2012.

[25] Metcalf HJ, van der Straten P. Laser Cooling and Trapping. Springer New York;.

[26] Steck DA. Rubidium 87 D Line Data; 2019.

[27] Kasevich M, Weiss DS, Riis E, Moler K, Kasapi S, Chu S. Atomic velocity selection using stimulated Raman transitions. Physical Review Letters. 1991;66:2297.

[28] McGuirk J. High precision absolute gravity gradiometry with atom interferometry. Stanford University; 2002.

[29] Lamb A. Cold Atom Gravity Gradiometry for Field Applications. University of Birmingham; 2019.

[30] Pfeiffer. Metal Seals;. Available from: https://www.pfeiffer-vacuum.com/en/know-how/mechanical-components-in-vacuum/materials/sealing-materials/metal-seals/.

[31] Zhu L, Lien YH, Hinton A, Niggebaum A, Rammeloo C, Bongs K, et al. Application of optical single-sideband laser in Raman atom interferometry. Opt Express. 2018;26:6542.

[32] Madkhaly SH, Coles LA, Morley C, Colquhoun CD, Fromhold TM, Cooper N, et al. Performance-Optimized Components for Quantum Technologies via Additive Manufacturing. PRX Quantum. 2021;2:030326.

[33] Taborelli M. Cleaning and Surface Properties. arXiv;2006.01585.

[34] Gragido W, Molina D, Pirc J, Selby N. Blackhatonomics: An Inside Look at the Economics of Cybercrime. 1st ed. Syngress Publishing; 2012.

[35] Wu X, Pagel Z, Malek BS, Nguyen TH, Zi F, Scheirer DS, et al. Gravity surveys using a mobile atom interferometer. Science Advances. 2019;5:0800.

[36] Norrgard EB, Sitaraman N, Barry JF, McCarron DJ, Steinecker MH, DeMille D. In-vacuum scattered light reduction with cupric oxide surfaces for sensitive fluorescence detection. Rev Sci Instrum. 2016;87:053119.

[37] Grinham R, Chew A. A Review of Outgassing and Methods for its Reduction. App Sci and Convergence Tech. 2017;26:95.

[38] Redhead P. Ultrahigh vacuum pressure measurements: Limiting processes. J Vac Sci Technol A. 1987;5:3215.

[39] Patrick H, Hanssen L, Zeng J, Germer T. BRDF measurements of graphite used in high-temperature fixed point blackbody radiators: A multi-angle study at 405nm and 658nm. Metrologia. 2012;49:S81.

[40] Hinton A, Perea Ortiz M, Lamb A, Rammeloo C, Stray B, Voulazeris G, et al. A portable magneto-optical trap with prospects for atom interferometry in civil engineering. Philos Trans R Soc A. 2017;375:2099.